Geochemistry xxx (xxxx) xxx

Contents lists available at ScienceDirect

Geochemistry

journal homepage: www.elsevier.com/locate/chemer

Geochemical composition of dykes along the Cameroon Line (CL): Petrogenesis and similarities with the Central Atlantic Magmatic Province

Asobo Nkengmatia Elvis Asaah [a,b,*], Tetsuya Yokoyama [a], Hikaru Iwamori [b], Festus Tongwa Aka [c], Jules Tamen [d], Takeshi Kuritani [e], Tomohiro Usui [f], Takeshi Hasegawa [g], Eric Martial Fozing [d]

[a] Department of Earth and Planetary Sciences, Tokyo Institute of Technology, 2–12–1, Ookayama, Meguro–Ku, Tokyo 152–8551, Japan
[b] Division of Earth and Planetary Material Sciences, Earthquake Research Institute, the University of Tokyo, 1–1–1 Yayoi, Bunkyo–ku, Tokyo 113–0032, Japan
[c] Department of Physical Sciences, School of Mathematics and Science, CCBC Essex Campus, 7201 Rossville Boulevard, Baltimore, MD 21237, USA
[d] Department of Earth Science, Faculty of Science, University of Dschang, P.O Box 07, Dschang, Cameroon
[e] Graduate School of Science, Hokkaido University, Sapporo 060–0810, Japan
[f] Department of Solar System Sciences, ISAS, JAXA, 3–1–1 Yoshinodai, Sagamihara, Kanagawa 252–5210, Japan
[g] Department of Earth Sciences, College of Science, Ibaraki University, 2–1–1 Bunkyo, Mito 310–8512, Japan

ARTICLE INFO

Handling Editor: Astrid Holzheid

Keywords:
Cameroon Line
Subalkaline dykes
Cameroon Volcanic Line
CAMP magmatism

ABSTRACT

We report whole-rock geochemistry and Sr–Nd–Pb isotopic compositions of mafic dykes intruded in the Precambrian granito-gneissic basement complex, exposed at Nyos, Batibo, Dschang and Foumban on the Cameroon Line. The dykes are alkaline (Batibo), transitional (Foumban), and subalkaline (Nyos, Batibo and Dschang) with SiO_2 of 45–54 wt% and MgO of 2–9 wt%, similar to dykes reported in other areas of the Cameroon Line (CL) and the Central Atlantic Magmatic Province (CAMP). The abundances of rare earth elements (REE) and the Primitive Mantle normalised patterns for the Nyos, Batibo and Dschang dykes are similar to those of MORB, indicating that the dykes formed at shallower depths by a higher degree of partial melting relative to the Foumban dykes and the alkaline lavas of the CL. The transitional basaltic dykes with steeper REE patterns have their sources at deeper levels in the lithospheric mantle, possibly the garnet-spinel transition zone and were generated by a lower degree partial melting of the lithospheric and plume components. The Nyos and Batibo subalkaline dykes show similar isotopic compositions with a spectrum extending from depleted (DMM-like) to enriched (EM1-like) mantle, indicating the similarity in their source components. The Dschang dykes show distinct isotopic characteristics with relatively unradiogenic Nd-Pb isotope compositions compared to the Batibo and Nyos dykes. The Foumban transitional dykes with characteristic wide ranges in Sr-Nd-Pb isotopic compositions reveal varying contributions from enriched mantle components (EM1 and EM2) in addition to its plume signature similar to those of CL lavas. The Nyos and Batibo dykes alongside other dykes on the CL have low TiO_2 abundances (<2 wt%), negative PM-normalised Nb-anomalies, and moderately to strongly enriched REE patterns, and isotopic composition that overlaps with those of CAMP, suggesting a similar lithospheric origin.

1. Introduction

The Cameroon Line (CL) comprises both oceanic and continental volcanic massifs (Cameroon Volcanic Line, CVL), minor intrusions (sills and dykes) and anorogenic plutonic complexes. Research on the CL has focused more on the volcanic massifs (Fitton and Dunlop, 1985; Halliday et al., 1990; Marzoli et al., 1999; Marzoli et al., 2000; Deruelle et al., 2007; Yokoyama et al., 2007; Aka et al., 2008; Kamgang et al., 2013; Njome and De Wit, 2014; Asaah et al., 2015a) and Precambrian plutonic basement complexes (Dumort, 1968; Tagne Kamga, 2003; Njonfang et al., 2006; Kwékam et al., 2010, 2013; Tchouankoué et al., 2016).

The CVL is a linear chain of Cenozoic-Recent volcanoes with similar geochemical characteristics, extending from the Island of Annobon in the Gulf of Guinea through the continent-ocean-boundary (COB) to mainland Africa (Fig. 1a; Fitton and Dunlop, 1985; Halliday et al., 1990). The source of these lavas has received much attention within the

* Corresponding author at: Department of Earth and Planetary Sciences, Tokyo Institute of Technology, 2–12–1, Ookayama, Meguro–Ku, Tokyo 152–8551, Japan.
E-mail addresses: asoboasaah@eri.u-tokyo.ac.jp, asoboasaah@gmail.com (A.N.E. Asaah).

https://doi.org/10.1016/j.chemer.2022.125865
Received 13 September 2021; Received in revised form 4 January 2022; Accepted 5 January 2022
Available online 15 January 2022

last four decades, from a purely asthenospheric source based on their trace element composition (Fitton and Dunlop, 1985) to a combination of asthenospheric and lithospheric sources based on their isotopic composition (Halliday et al., 1990; Deruelle et al., 2007; Yokoyama et al., 2007; Njome and De Wit, 2014; Asaah et al., 2015a, 2020, 2021).

Dykes occur in various geologic and tectonic settings, and their detailed study in space and time is indispensable in understanding several geological events (Aka et al., 2018). Most dykes are related to continental rifting. Dykes have a broad spectrum of chemical composition ranging from basic to felsic. However, mafic dykes are more

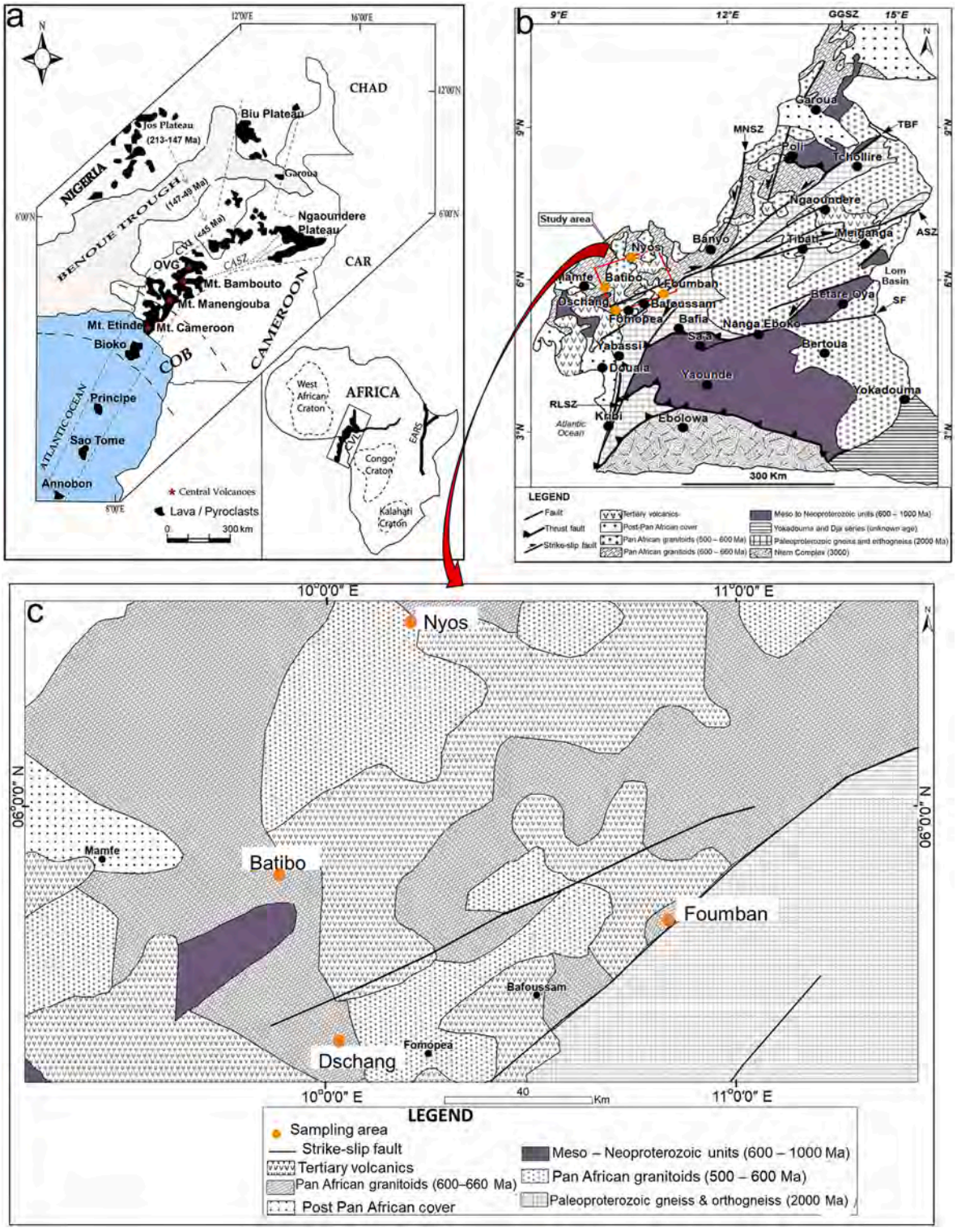

Fig. 1. Geologic map of the study area. a) presentation of the Cameroon Volcanic Line, b) Geologic and tectonic map of Cameroon, and c) Geologic map of the studied areas. Thick lines: shear zone (SZ); BSZ: Balche SZ; BNMB: Buffle Noir–Mayo Baleo; CCSZ: Central Cameroon SZ; GGSZ: Godé– Gormaya SZ; MNSZ: Mayo Nolti SZ; RLSZ: Rocher du Loup SZ; SSZ: Sanaga SZ.
Adapted from Asaah et al. (2015a) and Tchaptchet et al. (2017).

common and host useful information on magmatism and tectonism in the continental crust. Understanding the emplacement and geochemical composition of basaltic dykes along the CL has received less attention (Tchouankoue et al., 2012; Tchouankoue et al., 2014; Aka et al., 2018; Tchaptchet et al., 2017; Kouamo et al., 2019). Dykes and sills of basaltic composition with typical subalkaline/transitional character have been described in parts of the continental sector of the Cenozoic CVL (Ngounouno et al., 2001; Tchouankoue et al., 2012; Tchouankoue et al., 2014; Aka et al., 2018; Tchaptchet et al., 2017; Kouamo et al., 2019). For consistency and easy understanding, we limit the Cameroon Volcanic Line (CVL) to the Cenozoic volcanoes, while the CL comprises anorogenic plutonic complexes, Precambrian basement complex, dykes, sills and CVL developed on the Central Cameroon shear zone. The K-Ar (feldspar) ages of alkaline dykes (231.1 ± 4.8 Ma; Aka et al., 2018) and K-Ar (feldspar) and Ar-Ar (whole-rock) ages of subalkaline dykes (43–421 Ma; Ngounouno et al., 2001; Tchouankoue et al., 2014; Aka et al., 2018) on the CL are an indication that they are older than the Cenozoic volcanic activities of the CVL (Fitton and Dunlop, 1985; Marzoli et al., 2000; Aka et al., 2004; Kamgang et al., 2013). The major challenge remains a dense sampling and the generation of comprehensive petrological, geochemical and geochronological data to better understand their petrogenesis and tectonic relationship (Aka et al., 2018).

In this study, we use new geochemical and Sr–Nd–Pb isotope data for alkaline and subalkaline dykes from four locations in the continental sector of the CVL and CL to investigate their petrogenesis and constrain their relationship with CVL magmatism.

2. Regional tectonic setting and magmatism

The Cameroon Line (CL) is an important geologic structure in West Africa (Fitton and Dunlop, 1985; Halliday et al., 1988; Aka et al., 2004; Njome and de Wit, 2014; Merle et al., 2017) superimposed on the Central Cameroon shear zone (CCSZ; Browne and Fairhead, 1983; Fairhead, 1988). Unlike the Cameroon Volcanic Line (CVL) that consists of Cenozoic volcanoes aligned on the CCSV, the CL comprises anorogenic plutonic complexes, Precambrian basement complex, dykes, sills and CVL developed on this mega tectonic structure (Fig. 1b).

The Precambrian units outcropping in Cameroon are the 2883–3266 Ma Ntem complex (Takam et al., 2009), representing the northernmost part of the Congo Craton and the Neoproterozoic Pan African domain. The Precambrian domain of southwestern Cameroon was formed following the convergence and collision between the West African and Congo-São Francisco cratons along the Pan-African mobile belts (530–800 Ma: Meert and Voo, 1997; Ganwa et al., 2008; Penaye et al., 2004). The Precambrian in Cameroon was affected by N30° to N70°E striking shear zones, characterised by early transpressional tectonics followed by a transtensional regime (Ngako et al., 2003) that marked the final assembly of the Central African fold belt in Cameroon. Fractures act as pathways for Paleozoic and Mesozoic tholeiitic basalts thought to be related to the reactivation of the CCSZ in relation to the rifting and opening of the South Atlantic Ocean (Tchouankoue et al., 2014).

Other important magmatic structures adjacent to the CL include the Benue trough (BT) and the Jos Plateau (Fig. 1a insert). The earliest magmatism in the Jos plateau is represented by Norian (213 Ma) ring complexes (Bowden et al., 1976). Meanwhile, the oldest activity in the BT is Tithonian (147 Ma; Maluski et al., 1995). Recent studies have documented that the CL host older magmatic activities outcropping as dykes in the Nyos area (231.7 ± 4.8 Ma; Aka et al., 2018), Maham and Dschang (404.2 ± 3.51 Ma and 421.3 ± 3.5 Ma, respectively; Tchouankoue et al., 2014). Older dykes along the CL are thought to have been associated with the development of Silurian to Jurassic intracontinental rift systems in West Central Africa (Tchouankoue et al., 2014; Aka et al., 2018).

The magmatism of the Cameroon Line (CL) forming the older dykes, granitic plutons and the Cenozoic–recent alkaline basalts and subalkaline lavas (CVL magmatism) are comparable to the Mesozoic to recent volcanism in the Maranhao Plateau of Northeastern Brazil, which consists of subalkaline dykes (older) and alkaline lavas (younger). According to White and McKenzie (1989), if the geology of South America is compared to that of West Africa (Reconstruction of the central Atlantic region), the Mesozoic flood basalts of northeastern Brazil will lie in proximity to the diabase dykes of Liberia and the gabbro complex in Sierra Leone (Faure, 2001). Likewise, Mesozoic dolerite dykes in southeastern Nigeria have been interpreted to be related to the early stages of rifting during the formation of the Benue trough (Ekwueme, 1994; Coulon et al., 1996). Also, Mesozoic diabase sills and basaltic flows that outcrop along the east coast of North America recorded magmatic activities linked with the opening of the North Atlantic Ocean (Faure, 2001). Therefore, Mesozoic magmatism in the African plate was mainly associated with rifting of the continent. The dykes studied on the CL complements the gap in magmatic activity between the Precambrian basement, anorogenic complexes (73–30 Ma) (Guiraud et al., 1992; Lasserre, 1978) and the CVL (51 Ma–present; Aka et al., 2004; Fitton and Dunlop, 1985; Marzoli et al., 2000).

3. Sampling

Thirty samples from twelve basaltic dykes outcropping on the CL; Nyos area ($n = 2$), Batibo ($n = 4$), Dschang ($n = 2$) and Foumban ($n = 4$) were collected for this study (Fig. 1c). We also incorporated literature data for dykes studied from these areas (Tchouankoue et al., 2012; Tchouankoue et al., 2014; Tchaptchet et al., 2017; Aka et al., 2018; Kouamo et al., 2019). The dykes are mostly subalkaline or tholeiitic and alkaline, with an observable baked and chilled margin between the country rock and the dykes. The samples were collected from fresh portions at the centre of each dyke. The studied dykes outcrop as single dykes and composite dyke. Within the composite dyke, the contact between the subalkaline and alkaline dyke in the Batibo area was not easily distinguishable. The orientation of the dykes follows a general N30° to N80°E direction, similar to the direction of the CCSZ.

3.1. The Batibo dykes (Oku Volcanic Group)

The Batibo dykes are located in the Bamenda volcanic district of the Oku Volcanic Group or OVG (Asaah, 2015). Volcanic rocks in the Bamenda district range from primitive basanites and basalts to more evolved trachytes and rhyolites (Marzoli et al., 2000; Kamgang et al., 2013; Asaah et al., 2015a). Along the Bamenda-Mamfe highway, a series of exposed dykes (three dykes with one composite dyke) consisting of two alkaline dykes (OVG210-1 to OVG210-6 and OVG211-4&5) and two subalkaline dykes (OVG 211-2&3, OVG211-6 to OVG 211-9, and OVG212-1&2) were studied in the Batibo area (Fig. 2a & b, respectively). One of the subalkaline dyke occurs as a composite dyke with successive intrusions (Fig. 2b), which was intruded by one of the alkaline dyke. Field observation of the dykes indicates at least two emplacement sequences: a) the first stage involved the intrusion of a subalkaline dyke into the Precambrian basement, and b) the second stage involved the intrusion of an alkaline dyke into the subalkaline dyke. All samples from the Batibo dykes are fine to medium-grained and dark to grey in colour.

3.2. The Nyos dykes

The Nyos volcano is one of the stratovolcanoes that make up the Oku Volcanic Group (OVG) of the CVL. The Nyos volcano is typically composed of mafic volcanic rocks (basanite, basalt and trachy-basalt) with no felsic volcanic rocks reported (Aka et al., 2008, 2018; Asaah et al., 2015b; Hasegawa et al., 2019). The volcanic rocks host fresh peridotite xenoliths (Teitchou et al., 2011; Temdjim, 2012). Like the other volcanoes along the CVL, the volcanic rocks and dykes at Nyos erupted and cut through highly faulted Precambrian granitic basement rocks (Fig. 1b & c; Dunlop, 1983; Lasserre, 1978). Dykes in the Nyos area

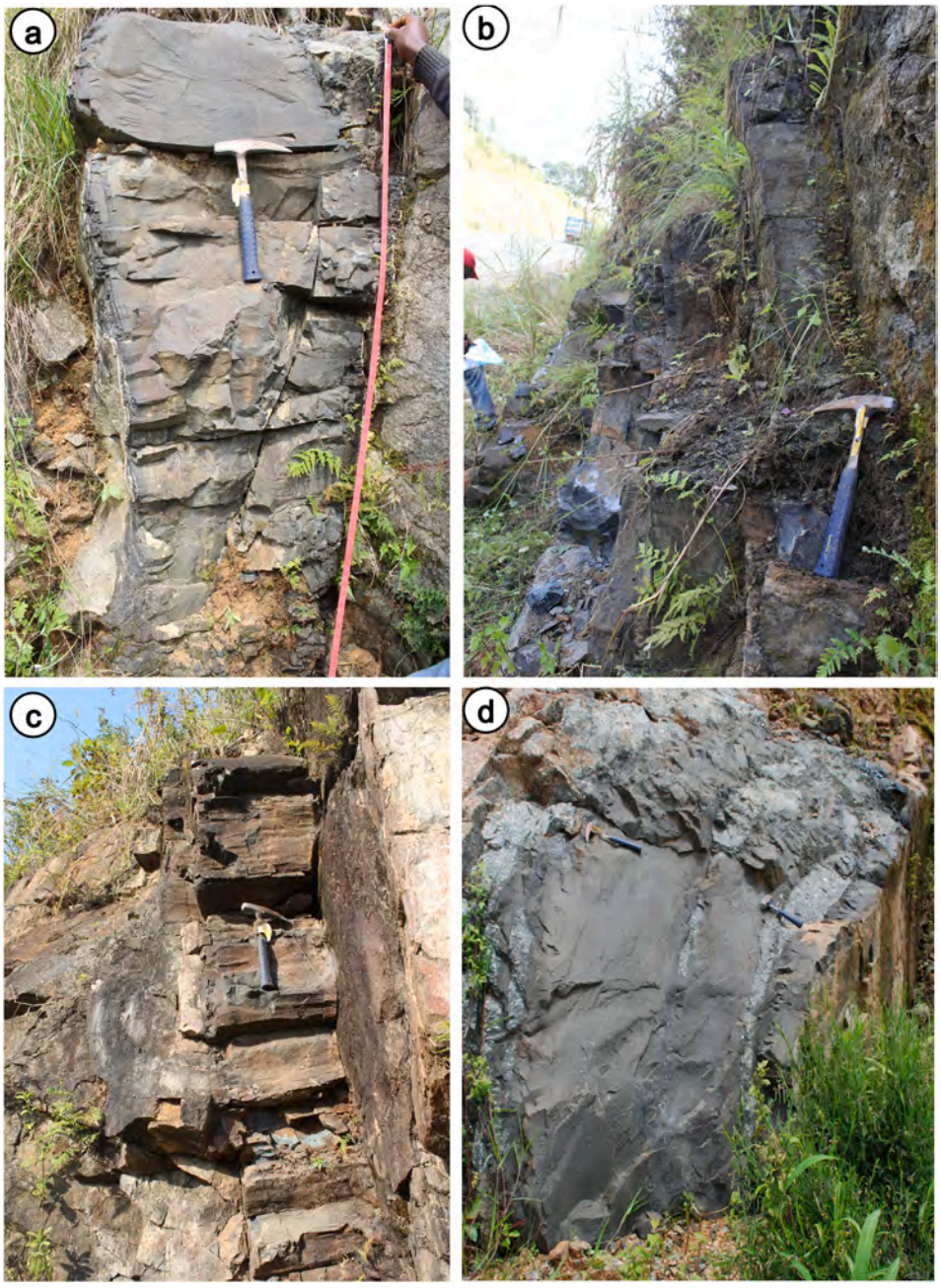

Fig. 2. Photographs of some outcrops in the localities studied. a) Batibo alkaline dyke, b) Batibo subalkaline dyke, c) Dschang dyke, and d) Foumban dyke.

outcrop (about 50 cm each in width) on the NE border of Lake Nyos and are vertically dipping with a N70°E trend and intrude the Terreneuvian quartz monzonite cliff. Samples were collected from two in-situ dykes ($n = 2$) and clasts ($n = 5$) of about 3–14 cm diameter around the lake. These clasts appear similar to the weathered surfaces of the in-situ dykes and are different from alkaline lavas at the macroscopic level.

3.3. The Dschang-Santcho and Foumban dykes (Mt. Bambouto)

Dschang is a locality on Mt. Bambouto, one of the major polygenetic volcanoes along the CVL. Volcanic products of Mt. Bambouto are lavas ranging in composition and character from basalts and basanites to more evolved trachyte, rhyolite, phonolites, and ignimbrites (Marzoli et al., 1999; Marzoli et al., 2000; Nkouathio et al., 2008; Kagou et al., 2010; Gountié Dedzo et al., 2012; Merle et al., 2017). Two dykes denoted DS1 and DS2 (DS referring to Dschang-Santcho) were sampled along the Dschang-Santcho escarpment located on the foot of Mt. Bambouto (Fig. 1c). The dykes cut through a granitic basement with partially assimilated basement materials observed in some portions of the dykes.

Foumban is a locality in the Noun plain of Mt. Bambouto. Like other volcanic fields of Mt. Bambouto, volcanic rocks in this area range from mafic to the felsic end members. Four mafic dykes ranging from 40 cm to 4 m in width, intruding granitic basements were sampled (Fig. 2d) along the Foumban-Ngaoundere highway.

4. Analytical methods

Samples for whole-rock analyses were jaw-crushed and chips of ~5 mm in diameter devoid of hammer and saw marks were handpicked. The jaw crusher was thoroughly cleaned with pressurised air followed by

deionised water after processing each sample. Selected chips were repeatedly washed with deionised water in an ultrasonic bath for 20 min. The final cleaning was done with acetone in an ultrasonic bath for 5 min. Samples were dried overnight at 110 °C. All samples were further checked for purity before pulverisation in an agate mill (FRITSCH planetary mill pulverisette 5). Rejected chips at this stage were first pulverised to clean the mill after first cleaning with reagent grade silicon dioxide.

Major elements and some minor elements, including Cr, Co, Ni, V and Sc, were analysed by X-ray fluorescence (XRF) spectrometry, using a Rigaku RIX 2100 at the Graduate School of Science Osaka City University in Japan. For the determination of 22 lithophile trace elements (Rb, Sr, Y, Cs, Ba, REEs, Pb, Th and U), ~50 mg of rock powders were digested using HF, HNO_3 and $HClO_4$ following the method described by Yokoyama et al. (1999). The abundances of these elements were determined with inductively coupled plasma mass spectrometry (ICP–MS; X–series II, Thermo–Fisher Scientific) at Tokyo Institute of Technology, Japan, by the calibration curve method with double internal standards (In + Tl) using a reference rock material JB–3 (basalt; Geological Survey of Japan) as the standard (Yokoyama et al., 2017). In addition, high field strength elements (HFSEs: Zr, Nb, Hf and Ta) were separately analysed following the method described in Makishima et al. (1999). Typical analytical precision (2σ) was 5% for Y and Ta, 4% for Nb and Pb, and <3% for the other trace elements.

Isotope analyses for Sr, Nd and Pb were performed using thermal ionisation mass spectrometry (TIMS) on a Triton *plus* (Thermo–Fisher Scientific) at Tokyo Institute of Technology. The ratios of $^{87}Sr/^{86}Sr$ and $^{143}Nd/^{144}Nd$ were corrected for internal mass fractionation using $^{86}Sr/^{88}Sr = 0.1194$ and $^{146}Nd/^{144}Nd = 0.7219$, respectively. Repeated analyses of standard materials NIST 987 (measured value: $^{87}Sr/^{86}Sr = 0.710264 \pm 3$) and JNdi–1 (measured value: $^{143}Nd/^{144}Nd = 0.512108 \pm 1$) was used to correct the results for Sr and Nd, respectively. Measurements of these standards were carried out during the same analytical period and were finally normalised using the recommended values of $^{87}Sr/^{86}Sr = 0.71025$ (accepted NIST 987) and $^{143}Nd/^{144}Nd = 0.512115$ (Tanaka et al., 2000). Typical analytical reproducibility (2σ) was 0.005% for Sr and Nd. Lead isotope ratios were precisely measured by the standard "double spike method" using the ^{204}Pb-^{207}Pb spikes as described in Hamelin et al. (1985), Kuritani and Nakamura (2003) and Rudge et al. (2009). Typical analytical precision (2σ) for $^{206}Pb/^{204}Pb$, $^{207}Pb/^{204}Pb$ and $^{208}Pb/^{204}Pb$ were 0.01%.

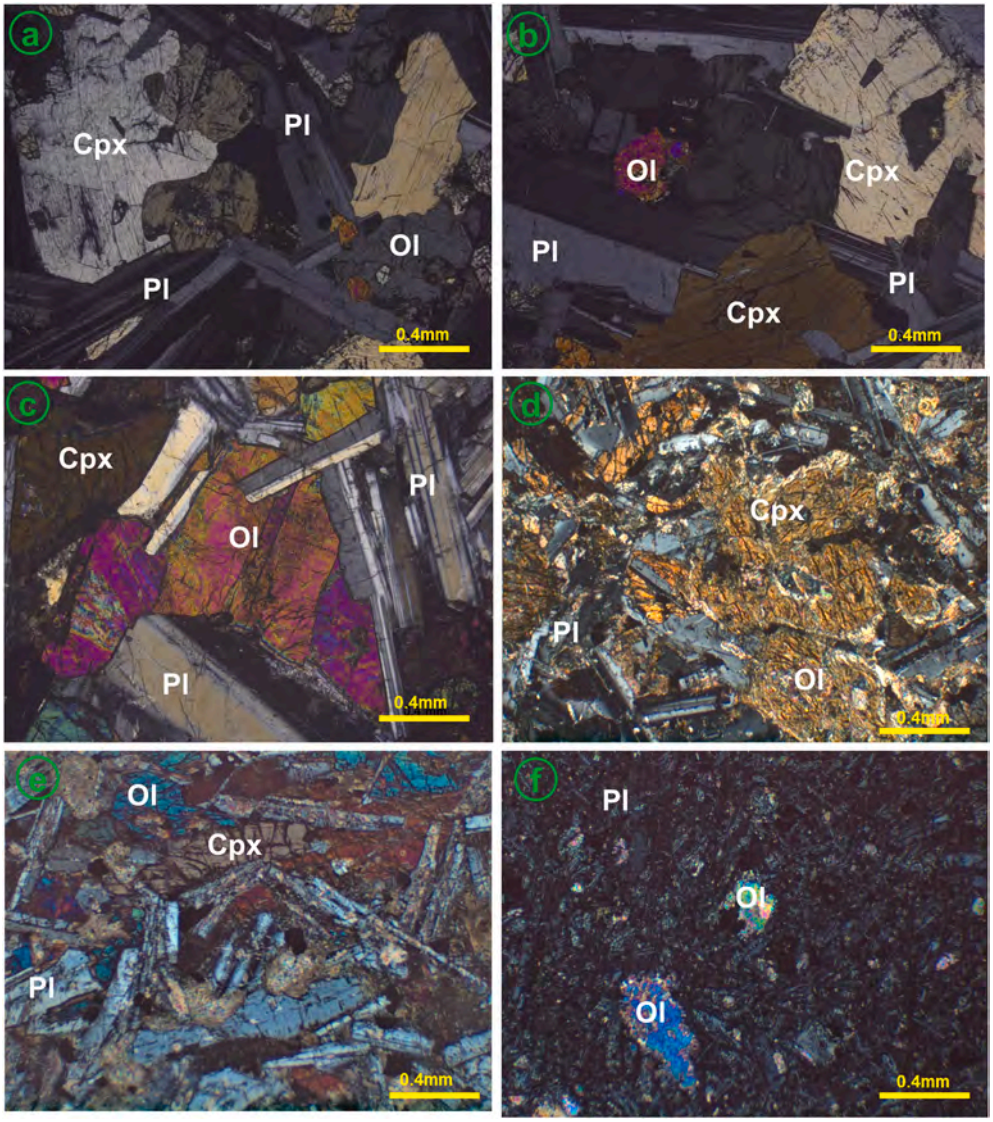

Fig. 3. Photomicrographs for representative samples of Nyos dyke (a &b), Batibo alkaline dykes (c & e), Dschang dyke (d), Batibo alkaline dyke.

Table 1
Major and trace elements compositions for dykes from Nyos, Batibo, Dschang and Foumban along the Cameroon Line.

	Nyos dykes							Batibo dykes							
	OVG17	OVG19	OVG26	OVG27	OVG29	OVG214	OVG217	OVG210-1	OVG210-2	OVG210-3	OVG210-4	OVG210-5	OVG210-6	OVG211-2	OVG211-3
SiO_2	49.8	49.9	50.1	49.4	49.5	48.5	50.0	45.5	42.2	42.2	44.2	41.6	43.2	47.3	47.6
TiO_2	1.35	1.41	1.55	1.38	1.39	1.71	1.16	3.10	2.88	3.02	3.00	2.85	2.93	1.58	1.59
Al_2O_3	15.6	15.1	15.0	14.8	15.9	16.1	15.5	15.8	15.2	15.3	15.5	15.0	15.5	14.6	14.9
Fe_2O_{3t}	13.1	13.8	14.2	13.9	13.2	12.1	13.3	13.8	14.2	14.4	13.7	12.2	10.9	13.4	13.2
MnO	0.17	0.18	0.18	0.18	0.16	0.16	0.17	0.233	0.181	0.260	0.263	0.214	0.202	0.170	0.145
MgO	7.47	7.60	7.12	7.80	7.06	8.34	8.08	2.08	3.25	2.09	2.09	2.38	1.73	8.22	7.46
CaO	9.50	9.21	9.52	9.17	9.35	6.95	9.39	6.75	9.27	8.99	8.33	11.6	11.0	8.83	8.88
Na_2O	2.94	2.96	2.99	2.92	3.05	2.31	3.01	2.95	3.54	3.11	3.20	3.77	3.45	2.73	2.70
K_2O	0.43	0.37	0.44	0.34	0.49	0.95	0.29	1.53	1.44	1.34	1.44	1.45	1.45	0.74	0.87
P_2O_5	0.14	0.14	0.16	0.13	0.15	0.38	0.11	2.85	2.70	2.89	2.77	2.65	2.68	0.20	0.20
Total	101	101	101	100	100	97.5	101	94.7	94.7	93.6	94.5	93.7	93.1	97.8	97.5
LOI	0.110	0.140	0.140	0.130	0.200	2.400	0.110	4.80	4.50	6.20	5.50	6.10	6.80	2.15	2.35
Cr	154	199	164	193	131	240	218	4.21	3.69	3.43	3.16	2.57	lld	233	235
Ni	162	186	141	192	156	146	201	lld	0.161	0.715	1.52	lld	lld	206	200
Co	54.4	57.0	51.6	55.8	52.1	49.0	56.5	11.4	17.1	20.4	12.7	15.6	12.8	54.6	56.0
V	173	188	190	192	164	179	174	63.5	58.0	67.5	58.6	55.7	59.0	191	195
Zn	103	110	116	109	103	100	102	211	154	207	216	177	229	106	107
Rb	11.4	8.19	10.2	6.89	12.1	52.3	7.2	26.3	19.9	22.2	24.3	19.5	23.2	23.6	29.6
Sr	230	193	242	202	240	487	203	1034	1439	1416	1266	1571	1440	300	312
Y	16.1	18.8	19.0	18.4	17.3	20.4	15.7	42.7	47.3	49.4	44.2	43.1	47.7	18.2	18.6
Zr	62.8	60.2	72.9	53.3	75.4	121.3	56.1	318	309	296	306	302	309	110	100
Nb	6.74	6.08	7.70	5.78	7.32	21.56	5.00	61.8	57.1	58.4	60.3	58.8	60.5	11.9	11.6
Cs	3.6	1.6	3.3	0.6	2.3	1.1	0.8	5.9	2.1	3.9	4.1	1.5	3.8	23.9	23.6
Ba	128	124	166	136	141	415	116	514	589	529	586	639	573	216	208
La	7.0	5.9	8.1	5.7	7.7	23.0	4.8	50.5	61.7	65.2	69.5	57.1	66.2	11.4	11.3
Ce	15.3	13.6	17.8	13.0	16.9	50.1	11.1	145	132	145	143	136	150	25	25
Pr	2.01	1.86	2.34	1.78	2.21	5.87	1.53	21.4	19.3	21.2	20.7	19.8	21.4	3.1	3.1
Nd	9.52	9.19	11.1	8.8	10.4	24.7	7.61	98.5	89.7	98.6	95.5	91.6	97.0	14.2	14.2
Sm	2.61	2.71	3.06	2.60	2.83	5.08	2.27	19.3	18.2	19.6	18.9	18.4	19.1	3.5	3.5
Eu	1.03	1.06	1.17	1.04	1.10	1.63	0.96	7.00	7.02	7.22	6.89	6.88	6.98	1.20	1.21
Gd	3.39	3.63	3.92	3.49	3.63	5.63	3.07	19.3	18.8	19.8	18.7	18.5	19.2	4.2	4.2
Tb	0.55	0.62	0.64	0.60	0.59	0.78	0.52	2.26	2.27	2.35	2.23	2.19	2.29	0.64	0.64
Dy	3.46	3.98	4.03	3.83	3.71	4.45	3.36	11.0	11.2	11.6	11.0	10.7	11.3	3.95	3.93
Ho	0.68	0.79	0.79	0.77	0.72	0.85	0.66	1.85	1.91	1.99	1.87	1.81	1.97	0.78	0.77
Er	1.83	2.14	2.13	2.08	1.96	2.31	1.81	4.51	4.66	4.91	4.55	4.47	4.94	2.12	2.10
Tm	0.25	0.29	0.29	0.29	0.26	0.31	0.25	0.51	0.53	0.55	0.52	0.51	0.58	0.29	0.29
Yb	1.56	1.86	1.82	1.80	1.67	1.98	1.57	2.93	3.09	3.20	3.04	3.05	3.42	1.84	1.81
Lu	0.23	0.27	0.27	0.27	0.24	0.29	0.23	0.39	0.43	0.44	0.42	0.41	0.47	0.27	0.26
Hf	1.82	1.84	2.10	1.59	2.21	3.28	1.68	7.38	7.29	6.95	7.20	7.00	7.22	2.92	2.75
Ta	0.37	0.33	0.44	0.32	0.40	1.18	0.26	3.17	3.01	2.98	3.10	3.04	3.08	0.58	0.56
Pb	1.87	1.03	1.62	1.00	1.54	2.58	0.88	1.31	2.35	2.98	1.63	1.90	2.25	1.61	1.60
Th	0.86	0.54	1.01	0.49	0.97	2.45	0.42	4.15	3.89	3.93	4.13	3.97	4.21	0.92	0.85
U	0.21	0.15	0.25	0.14	0.24	0.60	0.12	1.28	1.23	1.24	1.21	1.24	1.29	0.25	0.24

$Fe_2O_3/FeO = 0.15$

5. Results

5.1. Petrographic description

Photomicrographs of thin sections of representative samples of subalkaline dykes (Nyos and Batibo) and alkaline dykes (Batibo) are presented in Fig. 3. The subalkaline dykes are relatively fresh and present large (up to ~3 mm) holocrystalline aggregates of clinopyroxenes and plagioclase with few olivine crystals (Fig. 3a–e). The clinopyroxenes occur as large ophitic masses enclosing laths-shaped crystals of feldspars and microlites. The groundmass is formed by labradorite, thin olivine, augites and opaque oxide grains. Plagioclase and olivine phenocrysts are frequently altered to clay minerals and iddingsites. The olivine crystals are commonly enclosed in the clinopyroxene and stained brown with limonite, especially at its rims (Fig. 3). The large plagioclase crystals are almost equigranular with characteristic polysynthetic twinning. The alkaline samples are dark in colour, with phenocrysts of olivine, clinopyroxene and opaque minerals (<2 mm) spread in a fine-grained plagioclase dominated matrix (Fig. 3d). The olivine is altered to iddingsite, resulting in the characteristic cloudy and brownish colour under the microscope. Pyroxene, amphibole, magnetite, pyrite, and olivine with high iron content are commonly altered by oxidation to produce iron oxide minerals such as hematite and limonite. In contrast, plagioclase minerals commonly undergo hydrolysis to produce clay minerals.

5.2. Major elements

Major elements for samples from Nyos, Batibo, Dschang and Foumban dykes are presented in Table 1. The abundances of SiO_2 and MgO range from 45 to 54 and 2–9 wt%, respectively. Except for the samples of dyke OVG210 (OVG210–1 to OVG210–6) having a loss on ignition (LOI) ranging from 5 to 7 wt%, the samples from other dykes have LOI values less than 3.5. The total abundances of major elements have been recalculated to 100% on an anhydrous basis. Added to our plots are data from other dykes studied on the CL, including Dschang and Bangante (Tchouankoue et al., 2012), Manjo (Kouamo et al., 2019) and Kenkem (Tchaptchet et al., 2017). The samples plot in the fields of basanite, basalts, trachybasalts and basaltic trachy-andesite on the total alkaline versus silica diagram (Fig. 4) of Le Bas et al. (1986). Most of the samples (>80%) are subalkaline/transitional, while the remaining 20% are alkaline based on the classification by Irvine and Baragar (1971). All the samples analysed from Nyos are subalkaline. At the same time, some dykes in the Batibo area are alkaline, and others are subalkaline.

Batibo dykes									Dschang dykes		Foumban dykes				JB3 Split 9
OVG211-4	OVG211-5	OVG211-6a	OVG211-6b	OVG211-7	OVG211-8	OVG211-9	OVG212-1	OVG212-2	DS1	DS2	F2	F3	F4	F5	(average n=5)
45.0	45.5	47.3	47.2	47.3	47.8	48.0	47.1	47.9	48.2	47.4	48.1	52.7	48.3	52.6	51.2
2.98	2.99	1.59	1.77	1.52	1.68	1.82	1.61	1.75	1.44	1.48	1.92	1.77	2.09	1.82	1.45
15.3	15.5	14.7	16.2	14.8	15.4	16.9	14.9	15.9	15.6	14.9	16.2	15.6	15.5	15.7	17.3
12.5	12.1	12.9	13.2	12.7	11.8	13.0	12.0	12.3	12.7	12.0	11.4	10.4	12.0	10.5	12.0
0.236	0.310	0.148	0.145	0.151	0.145	0.166	0.153	0.155	0.187	0.172	0.16	0.14	0.17	0.15	0.18
4.79	4.89	7.37	7.97	7.98	7.01	8.42	6.87	6.76	7.37	8.10	7.20	4.40	6.73	4.54	5.20
7.77	7.56	9.29	7.11	9.14	9.42	5.47	10.09	9.13	9.65	9.56	8.05	6.58	7.60	6.29	9.84
3.72	3.83	2.78	2.68	2.83	2.85	2.78	2.73	2.87	2.39	2.32	2.80	2.43	3.19	3.22	2.74
1.54	1.57	0.89	0.66	0.74	0.75	0.66	0.83	0.62	0.77	1.03	2.18	3.42	1.92	3.06	0.79
2.76	2.70	0.21	0.23	0.20	0.22	0.24	0.21	0.23	0.22	0.24	0.47	0.62	0.62	0.63	0.29
96.7	97.0	97.1	97.2	97.4	97.1	97.4	96.5	97.7	98.6	97.3	98.5	98.0	98.2	98.4	101
3.20	3.10	2.75	2.68	2.61	2.85	2.80	3.52	2.35	1.30	2.60	1.85	2.40	1.97	1.62	
1.53	3.36	228	262	246	246	281	237	250	326	330	160	80.9	155	90.0	64.6
2.28	lld	210	230	233	241	284	202	204	105	167	135	60.9	122	64.9	36.8
17.5	18.9	54.1	65.0	59.9	61.2	70.0	55.9	57.1	51.9	54.4	42.5	35.3	42.3	35.1	32.8
64.2	61.8	192	210	183	201	219	197	211	201.8	191	150	103	139	106	378
167	161	107	84.6	107	114	116	109	127	93.4	92.6	70.1	82.8	85.2	82.9	105.0
23.5	21.4	29.0	22.2	23.1	18.7	15.4	20.7	12.6	39.5	49.8	100	235	56.2	204	14.2
1353	1363	322	344	317	343	331	348	340	386	447	671	930	561	794	416
44.6	45.1	18.5	17.6	19.0	21.1	17.7	21.2	20.9	18.3	17.3	30.7	55.3	30.7	51.1	26.5
298	306	113	126	109	119	129	113	124	113	123	308	148	201	179	99.3
58.2	60.0	12.5	13.9	12.0	13.2	14.0	12.6	13.5	9.68	11.6	32.5	29.3	32.1	21.4	2.5
1.1	0.9	16.8	10.9	12.4	6.4	2.3	9.1	5.3	15.7	14.5	2.48	3.08	0.99	2.35	0.93
646	636	225	231	213	221	255	207	214	355	433	592	694	608	699	250
62.2	45.7	11.8	12.8	11.5	12.5	12.2	13.5	13.4	13.3	15.7	23.0	34.2	26.0	39.5	8.0
138	136	25.5	26.9	24.8	27.0	25.5	27.5	28.0	29.8	34.4	49.0	73.2	57.9	84.7	20.6
20.1	20.0	3.2	3.32	3.13	3.40	3.18	3.43	3.53	3.77	4.26	5.9	8.6	7.22	9.92	3.13
93.4	92.7	14.4	14.7	14.1	15.4	14.2	15.4	15.9	16.7	18.6	23.7	33.2	30.9	38.6	15.8
18.6	18.7	3.5	3.49	3.43	3.74	3.37	3.71	3.85	3.78	4.00	4.72	6.17	6.26	7.24	4.18
7.01	7.15	1.21	1.23	1.20	1.33	1.28	1.29	1.36	1.33	1.39	1.37	1.43	1.80	1.64	1.31
18.7	19.0	4.2	4.11	4.18	4.61	4.00	4.57	4.64	4.38	4.46	4.87	5.94	6.54	6.99	4.71
2.24	2.25	0.65	0.63	0.64	0.71	0.62	0.69	0.71	0.64	0.64	0.67	0.77	0.89	0.90	0.74
10.9	11.0	3.9	3.80	3.91	4.30	3.77	4.18	4.30	3.87	3.72	3.79	4.10	5.04	4.84	4.64
1.84	1.86	0.77	0.74	0.77	0.84	0.74	0.82	0.83	0.75	0.72	0.74	0.78	0.99	0.93	0.95
4.45	4.59	2.11	2.02	2.09	2.30	2.02	2.22	2.27	2.06	1.94	2.02	2.12	2.66	2.52	2.67
0.50	0.52	0.29	0.28	0.28	0.31	0.28	0.30	0.31	0.28	0.26	0.27	0.28	0.36	0.34	0.38
2.91	3.12	1.83	1.78	1.80	1.97	1.74	1.89	1.96	1.79	1.67	1.76	1.79	2.29	2.14	2.49
0.40	0.43	0.27	0.26	0.26	0.29	0.25	0.28	0.29	0.26	0.25	0.26	0.26	0.34	0.31	0.38
6.96	7.24	3.04	3.32	2.88	3.15	3.39	2.99	3.26	2.95	3.18	7.94	3.79	5.17	4.19	2.67
2.98	3.07	0.61	0.67	0.58	0.64	0.68	0.60	0.66	0.51	0.62	1.74	1.59	1.75	1.12	0.11
2.65	2.59	1.40	1.82	1.47	1.64	2.04	1.66	1.85	2.43	2.91	2.48	3.17	2.59	3.98	4.84
4.01	3.99	0.95	1.03	0.91	1.00	1.07	0.91	1.04	1.15	1.42	1.76	2.79	1.67	3.41	1.30
1.24	1.31	0.26	0.28	0.25	0.28	0.30	0.26	0.29	0.30	0.36	0.46	0.52	0.40	0.64	0.48

Interestingly, amongst all samples outcropping as composite dykes in the Batibo area, two samples (OVG211–4 and 211–5) are alkaline, while the others are subalkaline (OVG2011–2 & 3 and OVG211–6 to 2011–9). The Foumban dykes plot close to the alkaline/sub–alkaline discrimination line and is referred to as transitional basalts. On a plot of MgO (wt %) versus other major element oxides (Fig. 5), the compositions of Na_2O, K_2O, TiO_2 and P_2O_5 (wt%) show a negative correlation (Fig. 5a–d). SiO_2, Al_2O_3, CaO and MnO show no clear correlation with MgO (wt%; Fig. 5e–h). Most samples with MgO > 6 (wt%) show a high degree of clustering relative to those with MgO < 6 (wt%). The alkaline dykes of the Batibo area have higher concentrations in TiO_2 and P_2O_5 than the other dykes (Fig. 5c & d).

5.3. Trace elements

Results for minor elements and trace elements are presented in Table 1. Except for the Batibo alkaline dykes having low values of Cr, Ni, and Co (≤3.4, ≤2.8, and 11.4–20.4 ppm), all of the dykes (Batibo subalkaline dykes, Foumban, Dschang and Nyos) have high values of Cr, Ni and Co abundances (131–330, 105–284, and 35.1–70.0 ppm, respectively). Incompatible alkaline and alkaline-earth elements such as Ba, Sr, Rb are higher in the alkaline and transitional basaltic dykes than the subalkaline basaltic dykes. The abundances of Ni and Co (ppm) correlate positively with MgO wt% (Fig. 6a–b), while Ba, Sr, Zr and Th (ppm) abundances decrease with increasing MgO wt% (Fig. 6c–f).

On the Chondrite normalised (Sun and McDonough, 1989) rare earth plot (Fig. 7), the patterns for the dykes studied and average peridotite from the subcontinental lithospheric mantle (SCLM) beneath the CL indicate enrichment of light rare earth elements (LREE) relative to heavy rare earth elements (HREE). The alkaline dykes, like CVL alkaline basalts and OIBs, are also enriched in REEs compared to the subalkaline dykes. Except for some Foumban dykes showing slight negative anomaly, the other dykes do not present any significant Eu anomaly (Fig. 7a–f). Fig. 8 presents Primitive Mantle normalised multi-element patterns of the studied dykes. Also shown in this figure are the average values of OIB, E–MORB, N–MORB (Sun and McDonough, 1989), and average composition of the SCLM beneath the CL (Asaah, 2015; Tamen et al., 2015; Tedonkenfack et al., 2019). In addition, there are enrichments in large ion lithophile elements (LILE; e.g., Rb, Ba) and high field strength elements (HFSE; e.g., Nb, Ta, U, Th) that are incompatible relative to LREE. The alkaline dykes from Batibo and Foumban show patterns akin to CVL lavas and OIBs, though with some elemental variations (Fig. 8a & b). The patterns for the subalkaline dykes fall between the average compositions of OIB and E–MORB. Except for the alkaline

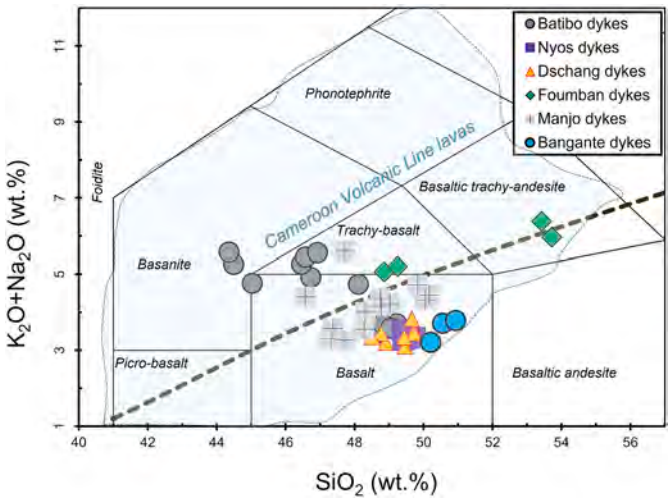

Fig. 4. (a) Total alkali versus silica classification diagram for the studied dykes. The dykes are alkaline, transitional to subalkaline in nature. The field for CVL is obtained from Asaah et al., 2015a and recently published data, including Wembenyui et al., 2020; Lemdjou et al., 2020; Asaah et al., 2021. Except otherwise stated, the same symbols and colours as used here will be used in subsequent diagrams. (For interpretation of the references to colour in this figure legend, the reader is referred to the web version of this article.)

dykes from Batibo with a pronounced negative K-Pb anomalies (Fig. 8a), all other dykes show variable positive K-Pb anomalies (Fig. 8b–f). In addition, all the Batibo subalkaline dykes and some samples from the Dschang and Nyos subalkaline dykes show slight negative Nb-Ta, while the rest of the dykes present positive Nb-Ta anomalies.

5.4. Sr–Nd–Pb isotopes

Sr–Nd–Pb isotope compositions for the dykes analysed in this study are presented in Table 2 and illustrated in Figs. 9 & 10. Available ages on CL dykes span a wide range; Dschang (421 Ma), Maham (404 Ma), Bangoua (241 & 149 Ma), Nyos (230 Ma), Kendem (192 Ma) and Bambouto (15 Ma). Initial isotopic ratios for our samples and those from other dykes (Dschang and Manjo) have been calculated based on available K-Ar and Ar/Ar age data (Tchouankoue et al., 2014; Aka et al., 2018). The assumed ages are considered because of their similarities in geochemical composition, orientation and proximity to the studied dykes. Isotope data for dykes from Nyos, Batibo, Foumban and Manjo were back-corrected at 225 Ma, while Dschang was back-corrected to 400 Ma. The Batibo alkaline dykes have $^{87}Sr/^{86}Sr_i$ and $^{143}Nd/^{144}Nd_i$ ratios ranging from 0.7039–0.7041 and 0.51250–0.51260, respectively. Initial $^{87}Sr/^{86}Sr_i$ and $^{143}Nd/^{144}Nd_i$ isotopic composition for subalkaline dykes from Batibo, Nyos, Dschang and Manjo range from 0.7027–0.7063 and 0.51110–0.51277, respectively, while those for the transitional basaltic dykes of Foumban range from 0.7059–0.7095 and 0.51194–0.51221, respectively. The initial $^{206}Pb/^{204}Pb_i$ isotopic composition range from 16.6 in a sample from Dschang to 19.9 in a sample from Manjo. On the $^{87}Sr/^{86}Sr_i$ vs $^{143}Nd/^{144}Nd_i$ isotopic space, most of the dykes plot in the lower half of the bulk silicate earth (BSE; Fig. 9a). The dykes form an array from the peridotite xenoliths beneath the CL, passing through EM1 to EM2. All the dykes plot above the Northern Hemisphere Reference Line (NHRL) of Hart (1984) on the $^{206}Pb/^{204}Pb_i$ versus $^{207}Pb/^{204}Pb_i$ isotope space diagram (Fig. 9b). Some of the dykes from Manjo have compositions overlapping with mafic alkaline basaltic lavas of the CVL. The dykes plot primarily within the DMM–EM1–EM2 triangular space (Fig. 10a & b).

6. Discussions

6.1. Alteration and crustal contamination

The alkaline dykes have higher LOI (3–7 wt%) and lower MgO, Ni, Cr, and V abundances relative to the transitional and subalkaline dykes suggesting that the alkaline basalts might have undergone some degree of low-temperature alteration. Ratios of LILE/HFSE are good weathering indicators because the LILE are mobile while the HFSE are relatively immobile. Ratios of Rb/Zr, Ba/Zr, Rb/Nb and Rb/Th for the alkaline dykes (0.06–0.08, 1.6–2.2, 0.3–0.4, and 4.9–6.3, respectively) are lower than the average values for fresh CVL lavas (0.14, 2.3, 0.6, 7.5, respectively; Asaah et al., 2015a). In contrast, Rb/Zr, Ba/Zr, Rb/Nb and Rb/Th ratios for the subalkaline dykes are in most cases higher than those of the CVL alkaline basalts. The lower LILE/HFSE ratios for the alkaline basaltic dykes relative to CVL basaltic lavas corroborate the effect of weathering on the alkaline dykes. Based on this, the alkaline dykes would not be considered further in discussing mantle sources.

The insignificant role of crustal contamination of mafic alkaline lavas of the CVL has been emphasised (Asaah et al., 2015a). Most less evolved alkaline basaltic lavas of the CVL host mantle xenoliths, suggesting rapid magma ascent to the surface. Furthermore, CVL lavas are younger (Cenozoic) with a shorter eruption history compared to dykes on the CL (15–421.3 Ma; Ngounouno et al., 2001; Tchouankoue et al., 2014; Aka et al., 2018). Therefore, it is essential to examine the degree of crustal contamination in the dykes due to the slow speed of magma ascent and emplacement within the continental crust (Xiong et al., 2013). Previous studies have reported minor amounts of crustal contamination of CL dykes by the host granitic basement (Tchouankoue et al., 2012; Tchaptchet et al., 2017; Aka et al., 2018; Kouamo et al., 2019). The ratios for Ce/Pb in the subalkaline dykes (Nyos, Batibo, Dschang, Kenkem and Bangante; 7–21) and transitional basaltic dykes of Foumban (20−23) are lower than average values obtained from CVL basaltic lavas (25–32), MORB and OIB (25 ± 5, Hofmann et al., 1986), but higher than average upper-crust (3.2, Taylor and McLennan, 1985) and CVL granitic basement (6.0; Asaah, 2015).

The subalkaline and transitional basaltic dykes show enrichments in the most incompatible elements relative to the more compatible HFSE and have relative depletions in Th ($(Th/La)_N = 0.2–1.0$). In addition, the dykes present variable Nb and Ti anomalies ($Nb_N/(Th_N + La_N)^2$ and $Ti_N/(Sm_N + Gd_N)^2$, respectively; Fig. 11). Some Nyos and Dschang dykes with no correlation in SiO_2 vs $^{87}Sr/^{86}Sr_i$ diagram (Fig. 11a) have negative Nb and Ti anomalies (Fig. 11b). The isotopic and trace element composition of the alkaline dykes with positive K–Pb–Sr spikes on the PM normalised multi-element plot (Fig. 8) is typical of most contaminated basaltic lavas. However, most subalkaline dykes present positive Nb-Ta spikes, inconsistent with crustal contamination. This implies that the positive K–Pb–Sr characteristics of the subalkaline dykes are a source characteristic requiring another means of enriching mantle-derived melts other than contamination. Therefore, the trace elements and isotopic composition of the subalkaline and transitional basaltic dykes, characteristically identical to arc lavas (subduction-related), have received minor post magmatic modification from the continental crust. Similar observations have been reported in CAMP basaltic dykes and are typical of lithospheric melting (Marzoli et al., 2018). The few subalkaline dykes with slight negative Nb-Ta anomalies would have received less than 10% crustal contamination, which in most cases is insignificant (Marzoli et al., 2018). On the other hand, the Batibo alkaline dykes present significant negative Nb-Ta anomalies suggestive of a greater amount of crustal contamination (possibly >20%). Based on the degree of weathering and the significant crustal contamination of the Nyos alkaline dykes, they would not be considered further in discussing mantle sources.

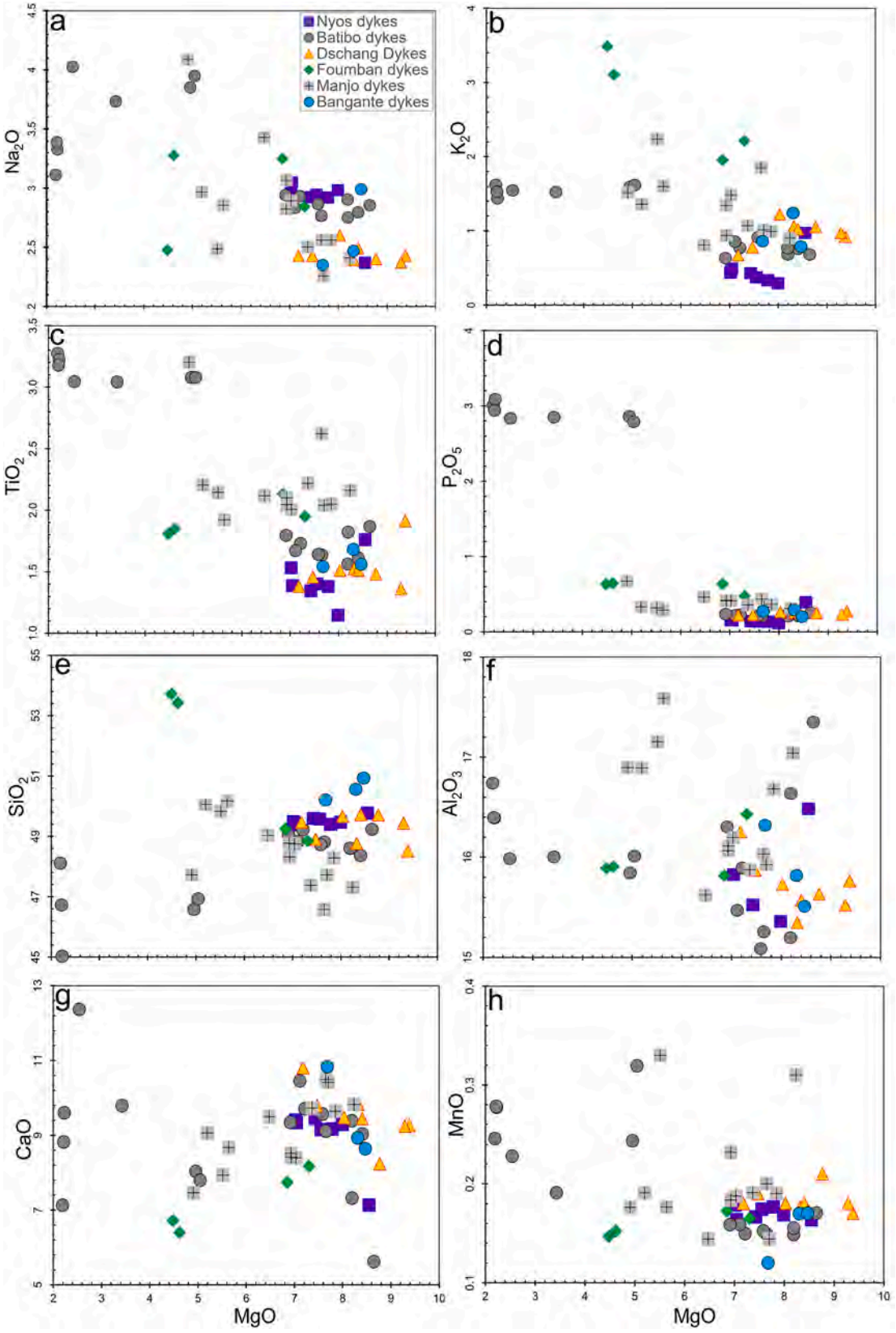

Fig. 5. Selected major element oxides (wt%) of the studied dykes along the CL plotted against MgO (wt%).

6.2. *Fractional crystallisation*

The majority of the subalkaline and transitional basaltic dykes studied have a restricted range in MgO (7–9 wt%). In addition, the abundances of Cr, Ni, and Co of the transitional (59–160 ppm, 61–134 ppm, and 35–43, respectively) and subalkaline (131–330 ppm, 105–284 ppm and 49–70 ppm, respectively) basaltic dykes are relatively lower than those assumed for the average composition of primary magma (Cr;

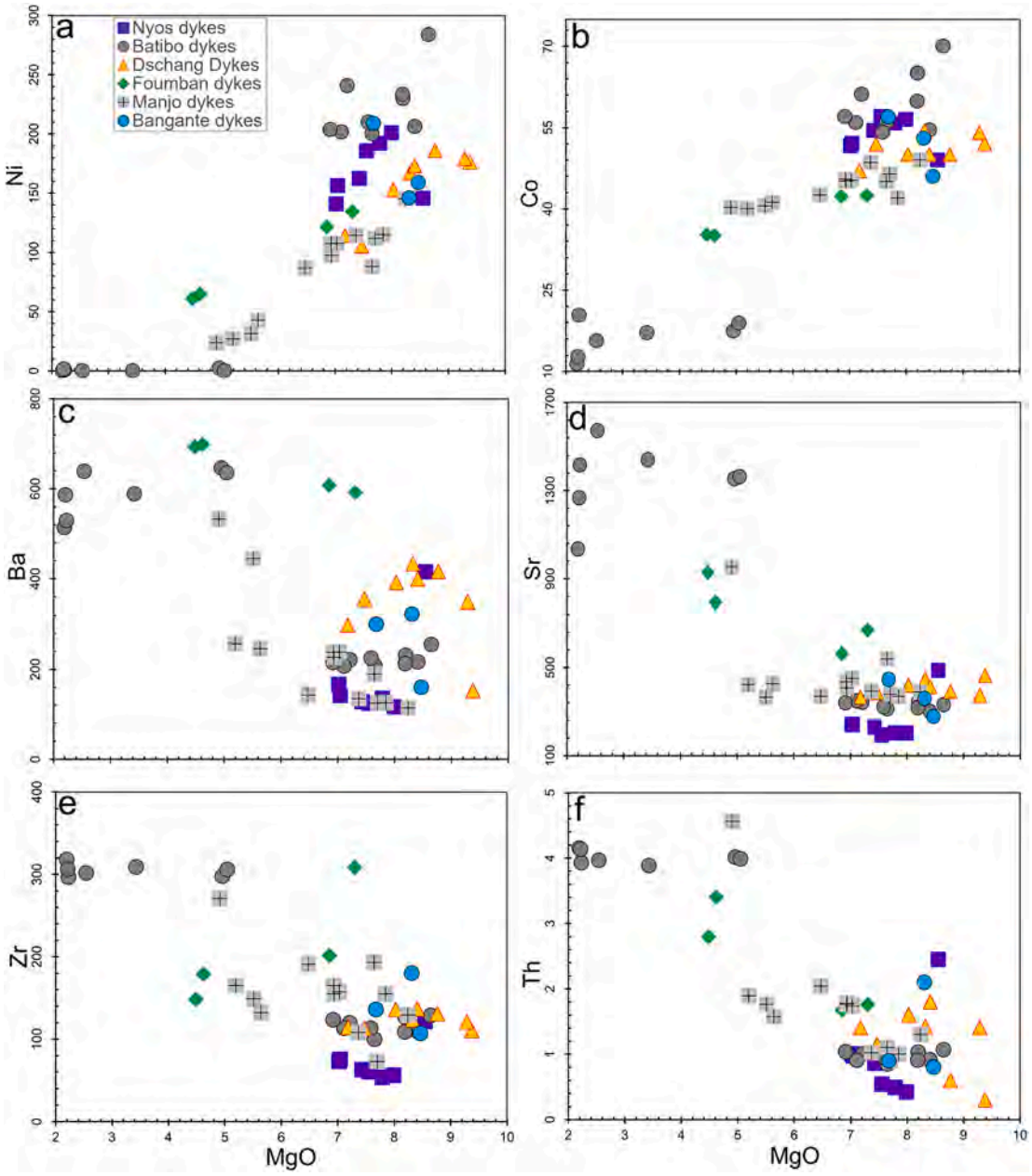

Fig. 6. Selected trace element (ppm) of the studied dykes along the CL plotted against MgO (wt%).

300–500 ppm, Ni; 300–400 ppm, Co; 50–70 ppm, Frey et al., 1978). These major elements and trace element characteristics suggest that the samples had undergone fractionation, with the subalkaline dykes being the least fractionated. The lack of high-Mg (primary) magmas is also common in the CVL lavas (Kamgang et al., 2013; Njome and de Wit, 2014; Asaah et al., 2015a, 2015b, 2020). Less than 5% of published data for CVL lavas have compositions with MgO (10–16 wt%), Ni, Cr and Co closed to pristine mantle composition (Njome and de Wit, 2014; Asaah et al., 2015a, 2015b, 2020, 2021; Gountié Dedzo et al., 2019; Wembenyui et al., 2020). The presence of these high-Mg lavas along the CVL is evidence of the involvement of a standard hot mantle (plume) source in the genesis of CVL magmas (Lees et al., 2020). At the same SiO_2 wt%, the subalkaline basaltic dykes have higher MgO wt% relative to CVL basaltic lavas, indicating differences in their sources and evolution. The positive correlation in plots of MgO versus Ni (Fig. 6a) and Cr (not shown) indicates the removal of mafic minerals like olivine and clinopyroxenes from the melt. Slight negative Eu anomaly in some dykes (Dschang, Foumban, Batibo and Bangangte) (Fig. 7) suggests the fractionation of plagioclase.

6.3. *Mantle source characterisation*

Basaltic magmas like those studied are either of asthenospheric or lithospheric origin. Differentiating their sources becomes more challenging in the Cameroon Line with basaltic lavas of varying compositions (alkaline, transitional and subalkaline).

Positive and negative slopes of REE patterns are widely considered a consequence of melting conditions and mantle source composition (Pearce, 2008). Inclined REE patterns as in OIB indicate low percentage melting, while flat patterns in MORB suggest a high degree of partial melting. The dykes studied present varying inclinations in REE patterns ranging from a more inclined pattern in the transitional basaltic dykes (Foumban) to an almost flat pattern in the subalkaline dykes (Nyos, Batibo, Dschang: Fig. 7). The nearly horizontal pattern in the subalkaline

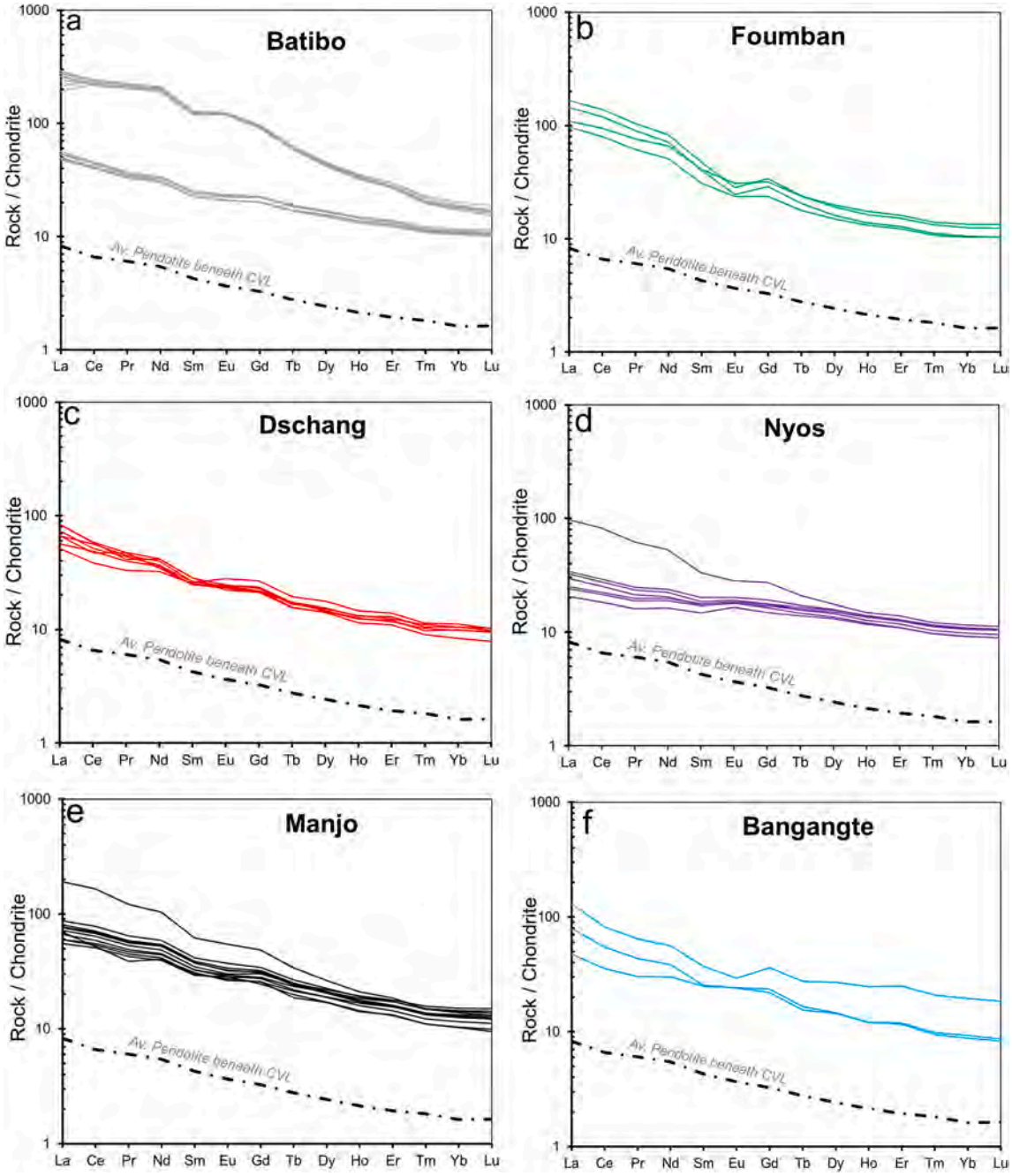

Fig. 7. Chondrite normalised REE diagrams for dykes studied along the CL. Data for average peridotites beneath the CVL is obtained from Lee et al., 1996; Tamen et al., 2007; Teitchou et al., 2011; Temdjim, 2012; Asaah, 2015; Tedonkenfack et al., 2019. Normalising values and data for OIB, N–MORB and E–MORB are from Sun and McDonough (1989).

dykes suggests their generation at shallow depth in the absence (or minimal presence) of garnet in the source since garnet has a strong HREE affinity and depletes these elements from the melts (Pearce, 2008). The absence of garnet in the source of these subalkaline dykes is supported by low $(Tb/Yb)_N$, La/Sm and La/Yb (1.51–1.74, 1.5–2.7 and 3.1–11.9) relative to the transitional basaltic dykes (1.73–1.92, 1.5–2.7 and 3.1–11.9, respectively). The $(La/Yb)_N$ ratios of the subalkaline dykes (2.3–6.7) are similar to the average $(La/Yb)_N$ ratio (5.1) for peridotites xenoliths believed to represent the composition of the lithospheric mantle (or upper non-convecting mantle or subcontinental lithospheric mantle, SCLM) beneath the CVL (Lee et al., 1996; Asaah, 2015; Tedonkenfack et al., 2019).

On the other hand, the transitional basaltic dykes with steeper REE patterns have their sources at deeper levels in the lithospheric mantle, possibly the garnet-spinel transition zone and were formed by lower degree partial melting similar to alkaline basaltic lavas of the CVL. Basaltic lavas derived from the lithospheric mantle are enriched in LILE and LREE with negative Nb-Ta anomalies. In contrast, those derived from the asthenospheric mantle have PM-normalised patterns like OIB, without negative Nb-Ta anomalies (Liao et al., 2014).

6.4. Mantle source components

It has been demonstrated that CVL magmatism is characterised by contributions from both the asthenosphere and the lithospheric mantle (Halliday et al., 1990; Yokoyama et al., 2007), involving at least three

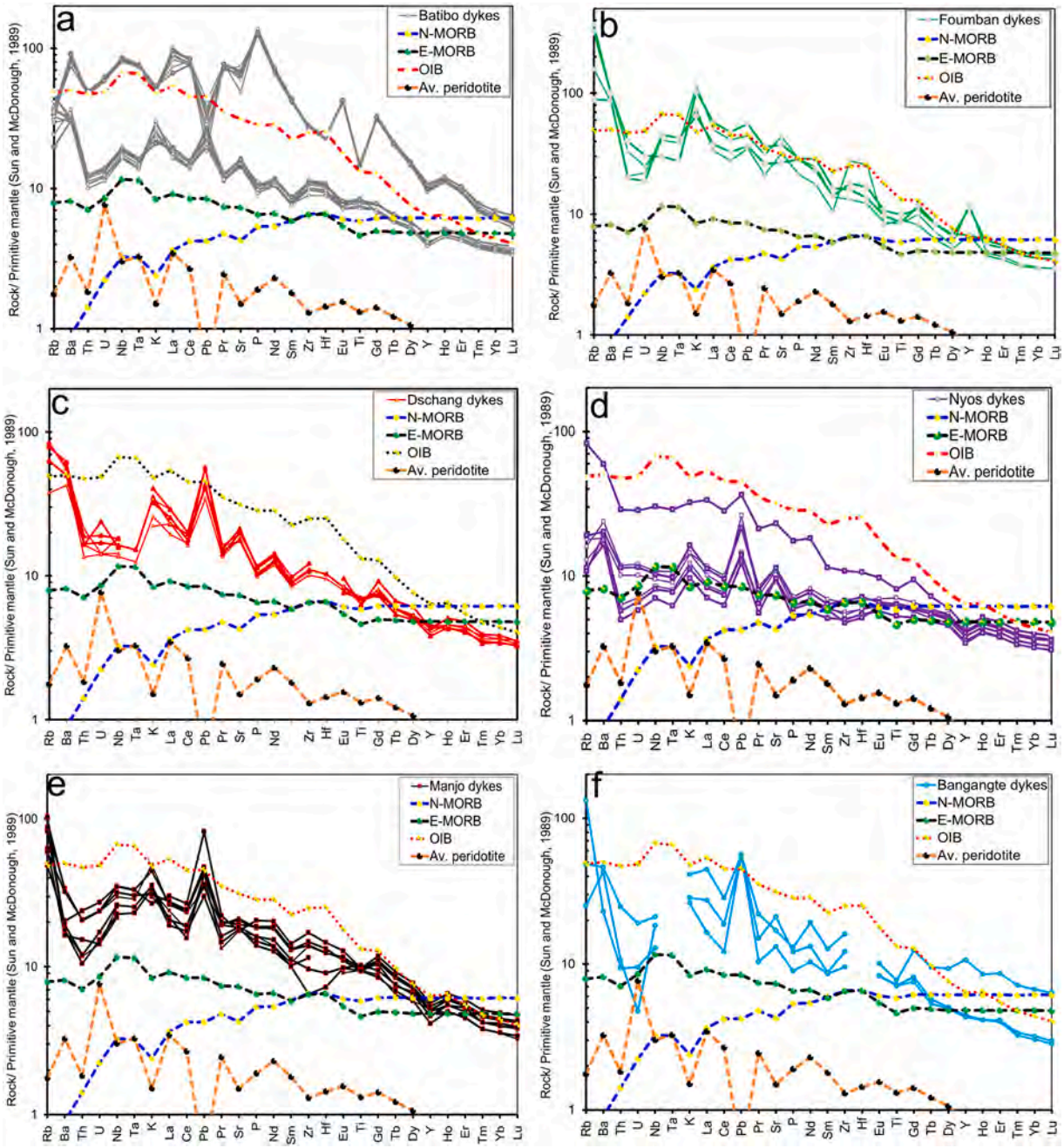

Fig. 8. Primitive Mantle normalised multi-element diagram for dykes studied along the CL. Data for average peridotites beneath the CVL is obtained from Lee et al., 1996; Tamen et al., 2007; Teitchou et al., 2011; Temdjim, 2012; Asaah, 2015; Tedonkenfack et al., 2019. Normalising values and data for OIB, N–MORB and E–MORB are from Sun and McDonough (1989).

mantle end members (Yokoyama et al., 2007; Kamgang et al., 2013; Asaah et al., 2015a, 2020). As trace elements, the isotopic composition also shows a disparity in the source of the dykes with the CVL magmatism. The subalkaline and transitional basaltic dykes are radiogenic in $^{87}Sr/^{86}Sr_i$ (mean; 0.7051 and 0.7079, respectively), unradiogenic in $^{143}Nd/^{144}Nd_i$ (mean; 0.5123 and 0.5120, respectively) and $^{206}Pb/^{204}Pb_i$ (18.93 and 18.02, respectively) relative to the CVL lavas ($^{87}Sr/^{86}Sr$ = 0.7033, $^{143}Nd/^{144}Nd$ = 0.51288 and $^{206}Pb/^{204}Pb$ = 19.85; Asaah et al., 2015a, 2021; Gountié Dedzo et al., 2019; Wembenyui et al., 2020; Lemdjou et al., 2020). At a first interpretation of the trace elements and isotopic composition of the dykes, one would think of a mixture of a plume-like (similar to CVL lavas) component with the continental crust to produce the dykes. However, the mixing of this nature would be characterised by significant Nb-Ta anomalies on the PM-normalised multi-element patterns for the dykes. Therefore, the hybrid isotopic composition in such mixing would have more radiogenic $^{87}Sr/^{86}Sr_i$ and unradiogenic $^{143}Nd/^{144}Nd_i$ and $^{206}Pb/^{204}Pb_i$ compared to the actual composition of the studied dykes. This hypothesis might be reasonable for the alkaline and transitional basaltic dykes of the CL, where a small amount of crustal component is necessary to produce the observed trace elements and isotopic signatures. Unlike alkaline lavas of the CVL showing characteristic FOZO-like composition, with mixing HIMU–DMM–EM1 components, the subalkaline and transitional basaltic dykes show a dominantly mixing of DMM–EM1–EM2. The Nyos and Batibo subalkaline dykes show similar isotopic composition with dominance of EM1–DMM (Figs. 9 & 10), indicating similarity in their source components. Interestingly, both dykes are located in the Oku Volcanic Group (OVG) of the CVL.

Table 2
Measured Sr-Nd-Pb isotope data for Nyos, Batibo, Dschang and Foumban dykes and their calculated initial isotopic compositions.

		$^{87}Rb/^{86}Sr$	$^{87}Sr/^{86}Sr$	$^{87}Sr/^{86}Sri$	2σ	$^{147}Sm/^{144}Nd$	$^{143}Nd/^{144}Nd$	$^{143}Nd/^{144}Ndi$	2σ	$^{238}U/^{204}Pb$	$^{206}Pb/^{204}Pb$	$^{206}Pb/^{204}Pbi$	2σ	$^{207}Pb/^{204}Pb$	$^{207}Pb/^{204}Pbi$	2σ	$^{208}Pb/^{204}Pb$	2σ
Nyos dykes	OVG17	0.142977	0.704475	**0.704017**	0.000003	0.165950	0.512662	**0.512417**	0.000002	7.0084	17.9135	**17.6646**	0.0007	15.5232	**15.5106**	0.0002	38.1345	0.0017
	OVG26	0.121647	0.705176	**0.704787**	0.000006	0.167138	0.511349	**0.511103**	0.000008	9.6429	18.2471	**17.9046**	0.0002	15.7805	**15.7632**	0.0002	38.6881	0.0002
	OVG27	0.098489	0.704638	**0.704322**	0.000002	0.178763	0.512626	**0.512363**	0.000002	8.6017	17.8916	**17.5861**	0.0003	15.5201	**15.5047**	0.0002	37.8327	0.0025
	OVG217	0.103030	0.704230	**0.703900**	0.000001	0.180107	0.512728	**0.512463**	0.000005	8.5068	17.8811	**17.5790**	0.0002	15.5095	**15.4942**	0.0005	37.8198	0.0017
Batibo dykes	*OVG210-5	0.035871	0.704242	**0.704127**	0.000003	0.121123	0.512780	**0.512602**	0.000006	40.2747	19.8826	**18.4520**	0.0003	15.7030	**15.6305**	0.0002	39.4876	0.0014
	OVG211-2	0.226898	0.705847	**0.705121**	0.000001	0.146439	0.512341	**0.512126**	0.000003	9.6891	17.9750	**17.6309**	0.0002	15.5954	**15.5780**	0.0019	38.1788	0.0080
	*OVG211-5	0.045282	0.704052	**0.703907**	0.000002	0.122175	0.512680	**0.512500**	0.000004	31.2558	19.7479	**18.6377**	0.0005	15.6716	**15.6154**	0.0003	39.3201	0.0015
	OVG211-7	0.210695	0.705872	**0.705197**	0.000002	0.146843	0.512346	**0.512130**	0.000002	10.5834	17.9304	**17.5545**	0.0007	15.5978	**15.5780**	0.0004	38.1221	0.0017
	OVG212-2	0.106962	0.705749	**0.705406**	0.000004	0.146682	0.512354	**0.512138**	0.000004									
Dschang dykes	DS1	0.295997	0.705636	**0.703949**	0.000018	0.136526	0.512256	**0.511898**	0.000002	7.4982	17.0331	**16.5531**	0.0003	15.4056	**15.3794**	0.0001	36.9232	0.0013
	DS2	0.321926	0.706543	**0.704709**	0.000001	0.130326	0.512235	**0.511894**	0.000003	7.5622	17.1769	**16.6928**	0.0001	15.4251	**15.3986**	0.0002	37.0674	0.0035
Foumban dykes	F2-a	0.430771	0.708050	**0.706671**	0.000007	0.120181	0.512391	**0.512214**	0.000007	11.4633	18.6487	**18.2416**	0.0004	15.6043	**15.5837**	0.0005	38.7367	0.0011
	F3-a	0.729828	0.711836	**0.709500**	0.000001	0.112313	0.512108	**0.511942**	0.000002	10.0955	18.1256	**17.7670**	0.0003	15.5869	**15.5687**	0.0004	39.1423	0.0012
	F4-a	0.289169	0.706811	**0.705886**	0.000003	0.122443	0.512223	**0.512043**	0.000002	9.4337	17.9986	**17.6635**	0.0001	15.5478	**15.5308**	0.0001	38.3943	0.0035
	F5-a	0.742022	0.711905	**0.709531**	0.000001	0.113259	0.512105	**0.511938**	0.000005	9.8918	18.7463	**18.3950**	0.0004	15.6348	**15.6170**	0.0002	39.8797	0.0015
Standard	JB3 (split 9)		0.703392		0.000004		0.513045		0.000004		18.2972		0.0003	15.5173		0.0002	38.1507	0.0018

Signifies alkaline dykes.
Measured standards.
JNdi-1: 0.512108 ± 1, NIST987: 0.710264 ± 3.

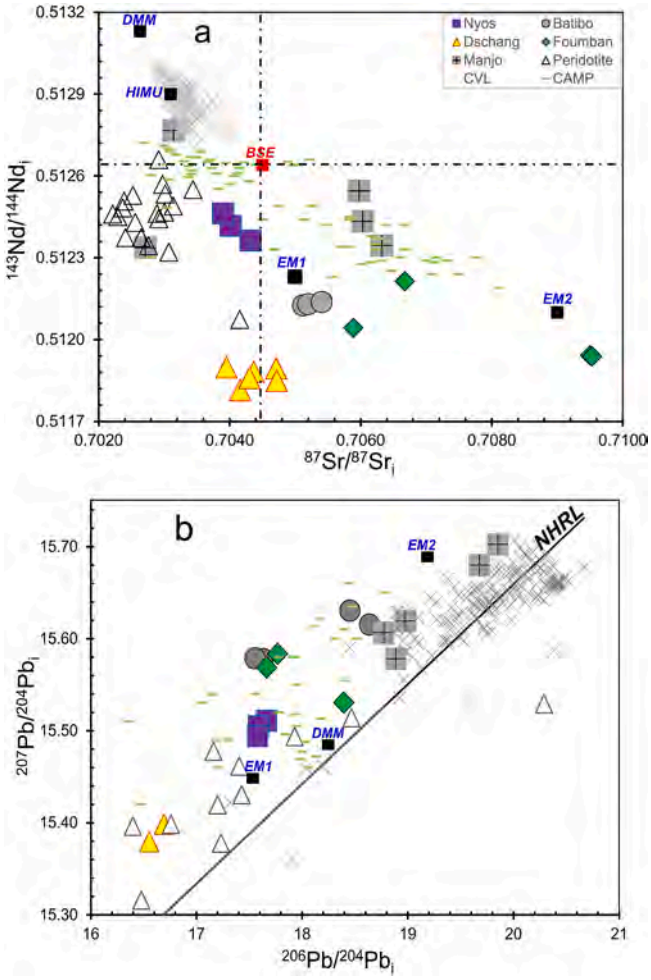

Fig. 9. (a) $^{143}Nd/^{144}Nd_i$ vs. $^{87}Sr/^{86}Sr_i$, and (b) $^{207}Pb/^{204}Pb_i$ vs. $^{206}Pb/^{204}Pb_i$. The initial ratios were calculated based on K-Ar, and Ar-Ar data for dykes reported in Tchounkoue et al., 2014; and Aka et al., 2018. Dykes from Nyos, Batibo, Foumban and Manjo were back corrected at 225 Ma, while Dschang dykes were back corrected at 400 Ma. The dykes plot below the BSE and above the NHRL. Sample OVG26 with $^{143}Nd/^{144}Nd_i$ (0.511103) is not plotted since it would reduce the scale. The Batibo alkaline dykes are not plotted in isotope space diagrams because of alteration and contamination discussed in the text. Literature data for CVL lavas is obtained from Asaah et al., 2015a and recently published data, including Wembenyui et al., 2020; Lemdjou et al., 2020; Asaah et al., 2021, while for peridotites is obtained from Asaah, 2015 and Lee et al., 1996.

The Dschang dykes show distinct isotopic characteristics with relatively unradiogenic Nd-Pb isotope compositions compared to the Batibo and Nyos dykes. Its composition showing a strong EM1 or crustal signature suggests melting recycled crustal material. The Foumban transitional basaltic dykes with characteristic wide ranges in Sr–Nd–Pb isotopic compositions reveals varying contributions from EM1 and EM2 in addition to its plume signature similar to those of CVL lavas.

The enriched signatures of the dykes studied are derived from recycled continental crustal materials (upper, lower or sediments) or SCLM veins introduced by metasomatism. Evidence of metasomatic activities on the SCLM beneath the CVL has been reported on peridotite xenoliths and basaltic lavas (Teitchou et al., 2011; Temdjim, 2012; Tchouankoue et al., 2012; Tchouankoue et al., 2014; Aka et al., 2018; Tchaptchet et al., 2017; Kouamo et al., 2019; Tedonkenfack et al., 2019; Asaah et al., 2021). The effects of metasomatism are more pronounced in the Manjo dykes, presenting radiogenic $^{206}Pb/^{204}Pb$ relative to the other dykes along the CVL. The recycled crustal material might have been introduced into the shallow mantle during the Paleozoic or

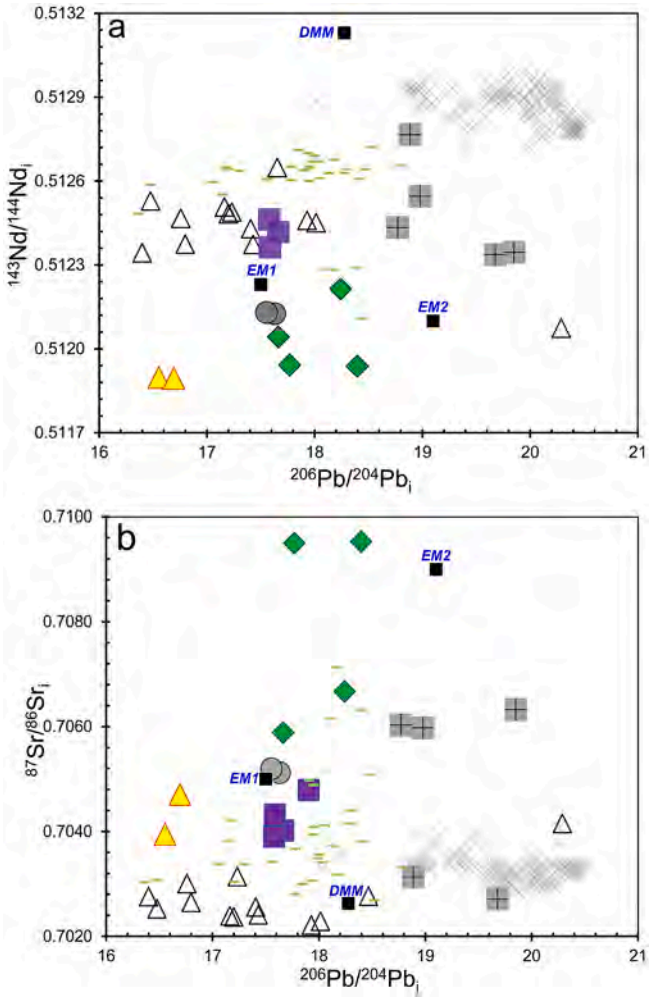

Fig. 10. a) $^{206}Pb/^{204}Pb$ versus $^{87}Sr/^{86}Sr$ and b) $^{206}Pb/^{204}Pb$ versus $^{143}Nd/^{144}Nd$ isotope plots for dykes on the CL. Sample OVG26 with $^{143}Nd/^{144}Nd_i$ (0.511103) is not plotted since it would reduce the scale. The Batibo alkaline dykes are not plotted in isotope space diagrams because of alteration and contamination discussed in the text. The source for literature data is the same as Fig. 9.

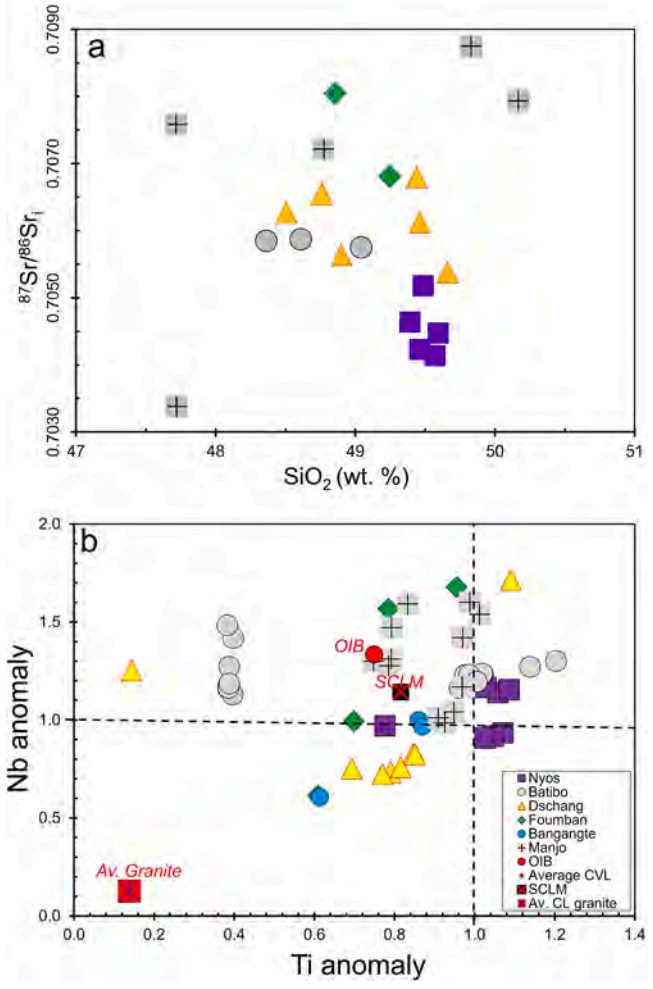

Fig. 11. Plots of a) $^{87}Sr/^{86}Sr$ versus SiO_2 (wt%) and b) Nb anomaly versus Ti anomaly. Most of the dykes do not show a clear correlation, especially when considered independently. The subalkaline dykes plot far from the average granitic composition of the CL, indicating a weak influence of crustal contamination.

Proterozoic subduction events (Marzoli et al., 2018).

6.5. Geochemical similarities with Central Atlantic Magmatic Province (CAMP)

Magmatism of the CL is represented by outcrops of varying ages corresponding to tectonic phases from the Neoproterozoic Pan African granites (620–420 Ma) constituting the basements to the Cenozoic effusive volcanics of the CVL (51 Ma–Present: Aka et al., 2018 and references therein). With available radioisotope ages for the oldest (Silurian; 421.3 ± 3.5 Ma; Tchouankoue et al., 2014) and youngest (149.2 ± 3.8 Ma; Tchouankoue et al., 2014) intrusive dykes on the CL, it is undoubtful that the magmatism of CL dykes covered a window of approximately 272 Ma. This period was contemporaneous with major magmatic activities in the Baborema province of NE Brazil (310 Ma-Present; Mizusaki et al., 2002), Central Atlantic Magmatic Province (CAMP, 189–207 Ma; Marzoli et al., 2018 and references therein) and the high–Ti basaltic dykes of the Carajás region of the Amazonian craton (199.3 ± 0.3 Ma; Giovanardi et al., 2019). The only available dykes with ^{40}Ar-^{39}Ar age for the CL plotting in the CAMP field is from Kenkem (Fig. 12; Tchouankoue et al., 2014).

Elemental and isotopic compositions of lavas from Nyos and Batibo

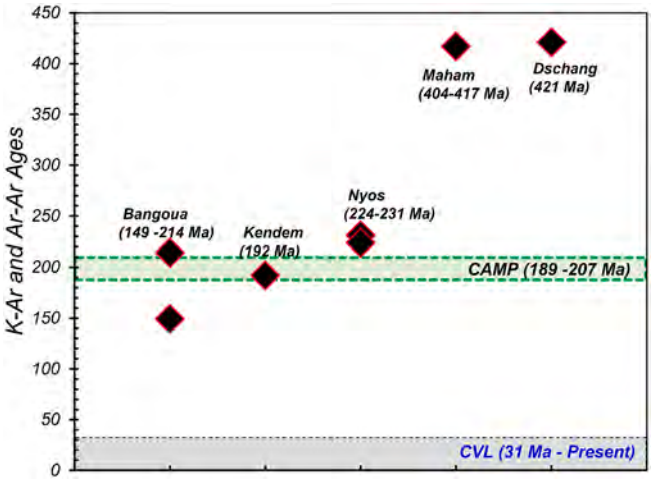

Fig. 12. Available K-Ar and Ar-Ar age data for dykes along the CL plotted and compared with CAMP and CVL.

are similar to those of the Kendem (Tchouankoue et al., 2014) and CAMP (Marzoli et al., 2018). The Nyos and Batibo with other dykes on the CL have low TiO_2 abundances (<2 wt%), negative PM-normalised Nb-anomalies, and moderately to strongly enriched REE patterns, similar to the dykes of the CAMP (Marzoli et al., 2018). Generally, dykes along the CL show depletions in HFSE and enrichments in LILE. In addition, the isotopic compositions of the Batibo and Nyos dykes overlap with those of the CAMP, suggesting similarities in source origin (SCLM) and evolution in time and space. It would be fascinating to investigate the absolute (precise Ar-Ar) ages of these two dykes to constrain their emplacement with CAMP activity. The Dschang dykes presenting different isotopic compositions to the Nyos and Batibo dykes, corroborates their emplacement before the CAMP activity.

Using available radioisotope data for the CL compiled in Aka et al. (2018), the magmatic and tectonic history can be reconstituted (Coulon et al., 1996). The Pan African orogeny that affected the Neoproterozoic granitic basement of the CL left behind fractures and zones of weaknesses (Toteu et al., 1987, 1990; Toteu et al., 2001; Tchaptchet et al., 2017) that have eased the emplacement of extrusive and intrusive magmatic rocks (Burke, 2001; Njonfang et al., 2011). The first phase of intrusion is characterised by dykes from Silurian to Jurassic (Vicat et al., 2001; Tchouankoue et al., 2012; Tchouankoue et al., 2014; Aka et al., 2018; Kouamo et al., 2019). The opening of the Equatorial Atlantic Ocean in the Cretaceous (96–130 Ma) was contemporaneous with magmatism in the Benue Trough (49–147 Ma: Wilson, 1992). The second phase of intrusive activity on the CL was more robust and characterised by the emplacement of numerous anaeorogenic plutonic complexes from late Cretaceous to Paleogene (30–73 Ma; Lasserre, 1966). The end of the second intrusive phase overlaps with the early Cenozoic volcanic activities of the CVL (31–Present; Fitton and Dunlop, 1985; Halliday et al., 1990; Marzoli et al., 1999; Marzoli et al., 2000; Aka et al., 2004, 2008; Njilah et al., 2004; Rankenburg et al., 2005; Kamgang et al., 2013; Asaah et al., 2015a).

7. Conclusion

Dykes of alkaline, transitional, and subalkaline affinities have been studied in Nyos, Batibo, Dschang and Foumban outcropping in exposed Neoproterozoic granito-gneissic basement complex of the Cameroon Line. Trace elements and isotopic compositions of the subalkaline and transitional basaltic dykes indicate they have received minor post magmatic modification from the continental crust. Most of the dykes studied have a restricted range in MgO (7–9 wt%), lower abundances in Cr, Ni, and Co, suggesting that the dykes were derived from fractionated melts. REE abundances and PM-normalised patterns for the subalkaline dykes are similar to MORB, indicating their formation at shallower depth by a higher degree of partial melting relative to the Foumban dykes and the alkaline lavas of the CVL. The transitional basaltic dykes with steeper REE patterns have their sources at deeper levels in the lithospheric mantle, possibly the garnet-spinel transition zone by lower degree partial melting of the lithospheric and plume components.

The Nyos and Batibo subalkaline dykes show similar isotopic compositions with dominance of EM1-DMM, indicating similarity in their source components. On the other hand, the Dschang dykes show distinct isotopic characteristics with relatively unradiogenic Nd-Pb isotope compositions compared to the Batibo and Nyos dykes. The Foumban transitional basaltic dykes with characteristic wide ranges in Sr-Nd-Pb isotopic compositions reveal varying contributions from EM1 and EM2 in addition to its plume signature similar to those of CVL lavas. The Nyos and Batibo dykes alongside other dykes on the CL have low TiO_2 abundances (<2 wt%), negative PM-normalised Nb-anomalies, and moderately to strongly enriched REE patterns. In addition, the isotopic compositions of the Batibo and Nyos dykes overlap with those of the CAMP, suggesting a similar source origin (SCLM). On the other hand, the Dschang dykes presenting different isotopic compositions to the Nyos and Batibo dykes corroborate their emplacement before the CAMP activity.

CRediT authorship contribution statement

Asobo Nkengmatia Elvis Asaah: Data curation, Formal analysis, Software, Investigation, Methodology, Visualization, Writing – original draft, Writing – review & editing. **Tetsuya Yokoyama:** Formal analysis, Funding acquisition, Project administration, Methodology, Resources, Software, Supervision, Validation, Writing – review & editing. **Hikaru Iwamori:** Formal analysis, Funding acquisition, Project administration, Resources, Software, Supervision, Validation, Writing – review & editing. **Festus Tongwa Aka:** Data curation, Investigation, Software, Visualization, Supervision, Writing – review & editing. **Jules Tamen:** Data curation, Investigation, Visualization, Writing – review & editing. **Takeshi Kuritani:** Data curation, Visualization, Methodology, Writing – review & editing. **Tomohiro Usui:** Data curation, Visualization, Methodology, Writing – review & editing. **Takeshi Hasegawa:** Data curation, Visualization, Methodology, Writing – review & editing. **Eric Martial Fozing:** Visualization, Writing – review & editing.

Declaration of competing interest

The authors declare that they have no known competing financial interests or personal relationships that could have appeared to influence the work reported in this paper.

Acknowledgements

This work was supported by JSPS KAKENHI grant numbers 26106002 and 26220713 to TY and 26247091 and 18H03747 to HI. In addition, material and financial support were provided by the Japan Science and Technology Agency (JST), Japan International Cooperation Agency (JICA). The first author is grateful for the opportunity to participate in the Long-term visiting program (November 2020–October 2021) organised by the Earthquake Research Institute (ERI), the University of Tokyo, where he received much support during the manuscript preparation. We thank the editors for proper handling and important observations to improve the previous version. Furthermore, comments and suggestions from Pr. Michiel de Kock, and an anonymous reviewer, significantly improved the quality of this contribution. ANEA, TY and HI also thank the members of the geochemistry laboratory in Tokyo Tech for collaboration during the analysis. ANEA also thank GERAS Cameroon for assistance during fieldwork.

References

Aka, F.T., Hasegawa, T., Nche, L.A., Asaah, A.N.E., Mimba, M.E., Teitchou, I., Ngwa, C., Miyabuchi, Y., Kobayashi, T., Kankeu, B., Yokoyama, T., Tanyileke, G., Ohba, T., Hell, J.V., Kusakabe, M., 2018. Upper triassic mafic dykes of Lake nyos, Cameroon (West Africa) I: K-ar age evidence within the context of Cameroon line magmatism and the tectonic significance. J. Afr. Earth Sci. 141, 49–59.

Aka, F.T., Yokoyama, T., Kusakabe, M., Nakamura, E., Tanyileke, G., Ateba, B., Ngako, V., Nnange, J., Hell, J.V., 2008. U-series dating of Lake nyos maar basalts, Cameroon (West Africa): implications for potential hazards on the Lake nyos dam. J. Volcanol. Geotherm. Res. 176 (2), 212–224.

Aka, F.T., Nagao, K., Kusakabe, M., Sumino, H., Tanyileke, G., Ateba, B., Hell, J., 2004. Symmetrical helium isotope distribution on the Cameroon volcanic line, West Africa. Chem. Geol. 203, 205–223.

Asaah, A.N.E., Yokoyama, T., Iwamori, H., Aka, F.T., Kuritani, T., Usui, T., Tamen, J., Hasegawa, T., Nche, L.A., Ohba, T., Gountié Dedzo, M., Chako Tchamabé, B., 2021. High–μ signature in lavas of Mt. Oku: Implications for lithospheric and asthenospheric contributions to the magmatism of the Cameroon Volcanic Line (West Africa). LITHOS 400–401 (2021), 106416.

Asaah, A.N.E., Yokoyama, T., Aka, F.T., Iwamori, H., Gountie, M.D., Tamen, T., Hasegawa, T., Usui, T., Fozing, E.M., Nche, A.L., 2020. Major/ trace elements and sr-nd-pb isotope systematics of lavas from lakes barombi mbo and barombi koto in the Kumba graben, Cameroon volcanic line: constraints on petrogenesis. J. Afr. Earth Sci. 161 (2020), 103675).

Asaah, A.N.E., Yokoyama, T., Aka, F.T., Usui, T., Wirmvem, M.J., Tchamabe, B.C., Ohba, T., Tanyileke, G., Hell, J.V., 2015a. A comparative review of petrogenetic processes beneath the Cameroon volcanic line: geochemical constraints. Geosci. Front. 6 (4), 557–570.

Asaah, A.N.E., Yokoyama, T., Aka, F.T., Usui, T., Kuritani, T., Wirmvem, M.J., Ohba, T., Tanyileke, G., Hell, J.V., 2015b. Geochemistry of lavas from maar-bearing volcanoes in the oku volcanic Group of the Cameroon Volcanic Line. Chem. Geol. 406, 55–69.

Asaah, A.N.E., 2015. In: Petrogenesis of Volcanic Rocks along the Cameroon Volcanic Line: Case of the Oku Volcanic Group, North-West Cameroon, Central Africa, Earth and Planetary Sciences. Tokyo Institute of Technology, Japan, p. 265.

Bowden, P., van Breemen, O., Hutchinson, J., Turner, D.C., 1976. Paleozoic and mesozoic age trends for some ring complexes in Niger and Nigeria. Nature 259, 297e299.

Browne, S., Fairhead, J.D., 1983. Gravity study of the central African rift system: a model of continental disruption 1. The ngaoundere and abu gabra rifts. Tectonophysics 94, 187e203.

Burke, 2001. Origin of the Cameroon Line of volcano-capped swells. J. Geol. 109, 349–362.

Coulon, C., Vidal, P., Dupuy, C., Baudin, P., Popoff, M., Maluski, H., Hermitte, D., 1996. The mesozoic to early cenozoic magmatism of the Benue trough (Nigeria); geochemical evidence for the involvement of the St. Helena plume. J. Petrol. 37, 1341–1358.

Ekwueme, B.N., 1994. Basaltic magmatism related to the early stages of rifting along the Benue trough: the obudu dolerites of south-East Nigeria. Geol. J. 29 (3), 269–276.

Deruelle, B., Ngounouno, I., Demaiffe, D., 2007. The Cameroon hot line (CHL): a unique example of an active alkaline intraplate structure in both oceanic and continental lithospheres. C. R Geosci. 339, 589–600.

Dumort, J.C., 1968. Notice explicative sur la feuille Douala-ouest et carte géologique de reconnaissance au 1:500 000. Bull. BRGM, 69 pages.

Dunlop, H., 1983. Strontium Isotope Geochemistry and Potassium-argon Studies on Volcanic Rocks From the Cameroon Line, West Africa. https://ethos.bl.uk/OrderDetails.do?uin=uk.bl.ethos.345758.

Fairhead, 1988. Mesozoic plate tectonic reconstructions of central SouthAtlantic Ocean: the role of West and Central Rift system. Tectonophysics 155, 181–191.

Faure, G., 2001. Origin of Igneous Rocks: The Isotopic Evidence. Springer Science & Business Media.

Fitton, J., Dunlop, H., 1985. The Cameroon line, West Africa, and its bearing on the origin of oceanic and continental alkali basalt. Earth Planet. Sci. Lett. 72, 23–38.

Frey, F., Green, D., Roy, S., 1978. Integrated models of basalt petrogenesis: a study of quartz tholeiites to olivine melilitites from South-Eastern Australia utilising geochemical and experimental petrological data. J. Petrol. 19, 463–513.

Ganwa, A.A., Frisch, W., Siebel, W., Ekodeck, G.E., Shang, C.K., Ngako, V., 2008. Archean inheritances in the pyroxene-amphibole bearing gneiss of the Méiganga area (Central North Cameroon): geochemical and 207Pb/206Pb age imprints. Compt. Rendus Geosci. 340, 211–222.

Giovanardi, T., Girardi, V.A.V., Teixeira, W., Mazzucchelli, M., 2019. Amazonian Craton: Sr-Nd isotopy, trace element geochemistry and inferences on their origin and geological settings. J. South American Earth Sciences 92 (June 2019), 197–208.

Gountié Dedzo, M., Asaah, A.N.E., Fozing, E.M., Chako Tchamabe, B., Zangmo, G.T., Dagwai, N., 2019. Petrology and geochemistry of lavas from Gawar, Minawao and Zamayvolcanoes of the northern segment of the Cameroon volcanic line (central Africa): constraints on mantle source and geochemical evolution. J. Afr. Earth Sci. 153 (2019), 31–41.

!"count(.//sb:host[1]//child::*//sb:date)">Guiraud, R., Binks, R., Fairhead, J., Wilson, M., . Chronology and geodynamic setting of 499 cretaceous-cenozoic rifting in west and Central Africa. Tectonophysics 213 (1), 227–234.

Gountié Dedzo, M., Njonfang, E., Kamgang, P., Nono, A., Zangmo Tefogoum, G., Kagou Dongmo, A., Nkouathio, D.G., 2012. Dynamic and evolution of the mounts bambouto and Bamenda calderas by the study of ignimbritic deposits (West-Cameroon, Cameroon Line). Syllabus Rev. Sci. Ser. 3, 11–23.

Hamelin, B., Manhes, G., Albarede, F., Allegre, C.J., 1985. Precise lead isotope measurements by the double spike technique: a reconsideration. Geochim. Cosmochim. Acta 49, 173–182.

Halliday, A.N., Davidson, J.P., Holden, P., DeWolf, C., Lee, D.-C., Fitton, J.G., 1990. Trace-element fractionation in plumes and the origin of HIMU mantle beneath the Cameroon line. Nature 347, 523–528.

Halliday, A.N., Dicken, A.P., Fallick, A.E., Fitton, J.D., 1988. Mantle dynamics: a Nd, Sr, Pb and Os isotopic study of the Cameroon volcanic line chain. J. Petrol. 29, 181–211.

Hart, S.R., 1984. A large-scale isotope anomaly in the southern hemisphere mantle. Nature 309, 753–757.

Hasegawa, T., Aka, F.T., Miyabuchi, Y., Nche, L.A., Kobayashi, T., Kaneko, K., Asaah, A. N.E., Kankeu, B., Issa, Ohba, T., Kusakabe, M., Hell, J.V., 2019. Eruption history and petrogenesis of rocks from Nyos volcano (NW Cameroon): evidence from lithostratigraphy and geochemistry. Journal of Volcanology and Geothermal Research 378 (2019), 51–71.

Hofmann, A.W., Jochum, K.P., Seufert, M., White, W.M., 1986. Nb and Pb in oceanic basalts; new constraints on mantle evolution. Earth Planet. Sci. Lett. 79, 33–45.

Irvine, T.N., Baragar, W.R.A., 1971. A guide to the chemical classification of the common volcanic rocks. Can. J. Earth Sci. 8, 523–548.

Kagou, D.A., Nkouathio, D., Pouclet, A., Bardintzeff, J.M., Wandji, P., Nono, A., Guillou, H., 2010. The discovery of late quaternary basalt on mount bambouto: implications for recent widespread volcanic activity in the southern Cameroon line. J. Afr. Earth Sci. 57, 96–108.

Kamgang, P., Chazot, G., Njonfang, E., Ngongang, N.B.T., Tchoua, F.M., 2013. Mantle sources and magma evolution beneath the Cameroon volcanic line: geochemistry of mafic rocks from the Bamenda Mountains (NW Cameroon). Gondwana Res. 24, 727–741.

Kouamo, N.-S.K., Tchatptchet, D.T., Ngueguim, A.L.T., Wambo, N.A.S., Tchouankoue, J. P., Cucciniello, C., 2019. Petrogenesis of basaltic dikes from the Manjo area (Western Cameroon): insights into the Paleozoic magmatism at the northern margin of the Congo craton in Cameroon. Arabian Journal of Geosciences 2019 (12), 281.

Kuritani, T., Nakamura, E., 2003. Highly precise and accurate isotopic analysis of small amounts of Pb using 205 Pb–204 Pb and 207 Pb-204 Pb, two double spikes. J. Anal. At. Spectrom. 18, 1464–1470.

Kwékam, M., Affaton, P., Bruguier, O., Liégeois, J.-P., Hartmann, G., Njonfang, E., 2013. The pan-African kekem gabbro-norite (West-Cameroon), U-Pb zircon age, geochemistry and Sr–Nd isotopes: geodynamical implication for the evolution of the central African fold belt. J. Afr. Earth Sci. 84, 70–88.

Kwékam, M., Liégeois, J.-P., Njonfang, E., Affaton, P., Hartmann, G., Tchoua, F., 2010. Nature, origin and significance of the Fomopéa pan-African high-K calc-alkaline plutonic complex in the central African fold belt (Cameroon). J. Afr. Earth Sci. 57, 79–95.

Lasserre, 1966. Confirmation de l'existence d'une séries de granites tertiaires au Cameroun. Bull. BRGM 3, 141–148.

Le Bas, M.J., Le Maitre, R., Streckeisen, A., Zanettin, B., 1986. A chemical classification of volcanic rocks based on the total alkali-silica diagram. J. Petrol. 27, 745–750.

Lasserre, M., 1978. Mise au point sue les granitoïdes dits "ultime" du Cameroun: gisement, petrographie et geochronologie. Bull. B.R.G.M 2 (IV), 143–159.

Lee, D.-C., Halliday, A.N., Davies, G.R., Essene, E.J., Fitton, J.G., Temdjim, R., 1996. Melt enrichment of shallow depleted mantle: a detailed petrological, trace element and isotopic study of mantle–derived xenoliths and megacrysts from the Cameroon line. J. Petrol. 37, 415–441.

Lees, M.E., John, F., Rudge, J.F., McKenzie, D., 2020. Gravity, topography, and melt generation rates from simple 3-D models of mantle convection. G-Cube. https://doi.org/10.1029/2019/GC008809.

Lemdjou, L.Y., Zhang, D., Tchouankoue, J.P., Hu, J., Ngongang, N.B.T., Tamehe, L.S., Yuan, Y., 2020. Elemental and Sr–Nd–Pb isotopic compositions, and K–Ar ages of transitional and alkaline plateau basalts from the eastern edge of the West Cameroon Highlands (Cameroon Volcanic Line). Lithos 358–359 (April 2020), 105414.

Liao, F., Zhang, L., Chen, N., Sun, M., Santosh, M., Wang, Q., Mustafa, H.A., 2014. Geochronology and geochemistry of meta-mafic dykes in the Quanji Massif, NW China: Paleoproterozoic evolution of the Tarim Craton and implications for the assembly of the Columbia supercontinent. Precambrian. Research 249 (August 2014), 33–56.

Makishima, A., Nakamura, E., Nakano, T., 1999. Determination of zirconium, niobium, hafnium and tantalum at ng g-1 levels in geological materials by direct nebulisation of sample HF solution into FI-ICP-MS. Geostand. Newslett. 23, 7–20.

Maluski, H., Coulon, C., Popoff, M., Baudin, P., 1995. 40Ar/39Ar chronology, petrology and geodynamic setting of mesozoic to early cenozoic magmatism from the Benue troughNigeria. J. Geol. Soc. London 152, 311–326.

Marzoli, A., Renne, P.R., Peccirillo, E.M., Castorina, F., Bellieni, G., Melfi, A.G., Nyobe, J. B., N'ni, J., 1999. Silicic magmas from the continental Cameroon Volcanic Line (Oku, Bambouto and Ngaoundere): 40Ar–39Ar dates, petrology, Sr–Nd–O isotopes and their petrogenetic significance. Contrib. Mineral. Petrol. 135 (133–150), 135.

Marzoli, A., Callegaro, S., Corso, D.J., Davies, J.H.F.L., Chiaradia, M., Youbi, N., Bertrand, H., Reisberg, L., Merle, R., Jourdan, F., 2018. The central Atlantic magmatic province (CAMP): a review. In: Tanner, L.H. (Ed.), The Late Triassic World, Topics in Geobiology, 46. https://doi.org/10.1007/978-3-319-68009-5_4.

Marzoli, A., Piccirillo, E., Renne, P., Bellieni, G., Iacumin, M., Nyobe, J., Tongwa, A., 2000. The Cameroon volcanic line revisited: petrogenesis of continental basaltic magmas from lithospheric and asthenospheric mantle sources. J. Petrol. 41, 87–109.

Meert, J.G., Voo, R.V.D., 1997. The Assembly of Gondwana 800-450 Ma. J. Geodymxmics 23 (314), 223–235.

Merle, R., Marzoli, A., Aka, F.T., Chiaradia, J.M., Reisberg, L., Castorina, F., Jourdan, F., Renne, P.R., N'ni, J., Nyobe, J.B., 2017. Mt Bambouto Volcano, Cameroon line: mantle source and differentiation of within-plate alkaline rocks. J. Petrol. 58, 933–962.

Mizusaki, A.M.P., Thomaz-Filho, A., Milani, E.J., De Césero, P., 2002. Mesozoic and Cenozoic igneous activity and its tectonic control in northeastern Brazil. Journal of South American Earth Science 15 (2), 183–198.

Ngako, V., Affaon, P., Nnange, J.M., Njanko, T., 2003. Pan-African tectonic evolution in central and southern Cameroon: transpression and transtension during sinistral shear movements. J. Afr. Earth Sci. 36, 207–214.

Ngounouno, I., Deruelle, B., Guiraud, R., Vicat, J.-P., 2001. Magmatismes tholeiitique et alcalin des demi-grabens cretaces de Mayo Oulo-Lere et de Babouri-Figuil (Nord du Cameroun–Sud du Tchad) en domaine d'extension continentale. C. R. Acad. Sci. Paris, Ser. IIa 333, 201–207.

Njilah, I.K., Ajonina, H.N., Kamgang, K.V., Tchinjang, M., 2004. K-Ar ages, mineralogy, major and trace element geochemistry of the Tertiary-Quatenary lavas from the Ndu Volcanic ridge NW Cameroon. Afr. J. Sci. Technol. 5, 47–56.

Njome, M.S., de Wit, M.J., 2014. The Cameroon line: analysis of an intraplate magmatic province transecting both oceanic and continental lithospheres: constraints, controversies and models. Earth Sci. Rev. 139, 168–194.

Njonfang, E., Ngako, V., Kwekam, M., Affaton, P., 2006. Calc-alkaline orthogneisses of the Foumban-bankim shear zone: witnesses of an internal zone of a pan-african active margin. Compt. Rendus Geosci. 338, 606–616.

Njonfang, E., Nono, A., Kamgang, P., Ngako, V., Tchoua, F.M., 2011. Cameroon linemagmatism (Central Africa): a reappraisal. In: Beccaluva, L., Bianchini, G., Wilson, M. (Eds.), Volcanism and Evolution of the African Lithosphere, GSA, Special Paper, 478, pp. 173–191.

Nkouathio, D.G., Kagou Dongmo, A., Bardintzeff, J.M., Wandji, P., Bellon, H., Pouclet, A., 2008. Evolution of volcanism in graben and horst structures along the cenozoic Cameroon line (Africa): implications for tectonic evolution and mantle source composition. Mineral. Petrol. 94, 287e303.

Pearce, J.A., 2008. Geochemical fingerprinting of oceanic basalts with applications to ophiolite classification and the search for Archean oceanic crust. Lithos 100, 14–48.
Penaye, J., Toteu, S.F., Tchameni, R., Van Schmus, W.R., Tchakounté, J., Ganwa, A., Miyem, D., Nsifa, E.N., 2004. The 2.1 ga west central African Belt in Cameroon: extension and evolution. J. Afr. Earth Sci. 39, 159–164.
Rankenburg, K., Lassiter, J.C., Brey, G., 2005. The role of continental crust and lithospheric mantle in the genesis of Cameroon Volcanic Line lavas: constraints from isotopic variations in lavas and megacrysts from Biu and Jos Plateaux. J. Petrol. 46 (1), 169–190.
Rudge, J.F., Reynolds, B.C., Bourdon, B., 2009. The double spike toolbox. Chem. Geol. 265, 420–431.
Sun, S.-S., McDonough, W., 1989. Chemical and isotopic systematics of oceanic basalts: implications for mantle composition and processes. Geol. Soc. Lond., Spec. Publ. 42, 313–345.
Tanaka, T., Togashi, S., Kamioka, H., Amakawa, H., Kagami, H., Hamamoto, T., Yuhara, M., Orihashi, Y., Yoneda, S., Shimizu, H., 2000. JNdi-1: a neodymium isotopic reference inconsistency with LaJolla neodymium. Chem. Geol. 168, 279–281.
Tagne Kamga, G., 2003. Petrogenesis of the neopoterozoic ngondo plutonic complex (Cameroun, west-Central Africa): a case of late collisional ferro-potassic magmatism. J. Afr. Earth Sci. 36, 149–171.
Takam, T., Arima, M., Kokonyangi, J., Daniel, J., Dunkley, D.J., Nsifa, Emmanuel N., 2009. Paleoarchaean charnockite in the Ntem Complex, Congo Craton, Cameroon: insights from SHRIMP zircon U-Pb ages. In: 104. J. of Mineralogical and Petrological Sciences, pp. 1–11.
Tamen, J., Nkoumbou, C., Mouafo, L., Reusser, E., Tchoua, F.M., 2007. Petrology and geochemistry of monogenetic volcanoes of the barombi koto volcanic field (Kumba graben, Cameroon volcanic line): implications for mantle source characteristics. Compt. Rendus Geosci. 339, 799–809.
Tamen, J., Nkoumbou, C., Reusser, E., Tchoua, F., 2015. Petrology and geochemistry ofmantle xenoliths from the Kapsiki plateau (Cameroon volcanic line): implications forlithospheric upwelling. J. Afr. Earth Sci. 101, 119–134.
Taylor, S.R., McLennan, S.M., 1985. The continental crust: Its composition and evolution. In: Blackwell Scientific Publications, Oxford, pp. 1–328.
Tchaptchet, T.D., Wambo Simeni, N.A., Keutchafo Kouamo, N.A., Tchouankoue, J.P., Cucciniello, C., 2017. Geology, mineralogy and geochemistry of the kekem dyke swarm (Western Cameroon): insights into paleozoic-mesozoic magmatism and geodynamic implications. Compt. Rendus Geosci. 349, 175–185.
Tchouankoue, J.P., Wambo, N.A.S., Kagou, D.A., Wörner, G., 2012. Petrology, geochemistry, and geodynamic implications of basaltic dyke swarms from the southern continental part of the Cameroon volcanic lineCentral Africa. The Open Geol. J. 6, 72–84.
Tchouankoue, J.P., Simeni Wambo, N.A., Kagou Dongmo, A., Li, X.H., 2014. 40Ar/39Ar dating of basaltic dyke swarm in WesternCameroon: evidence of Late Paleozoic and Mesozoic magmatism in the corridor of the Cameroon Line. J. Afr. Earth Sci. 93, 14–22.
Tchouankoué, J.P., Li, X., Ngo Belnoun, R.N., Mouafo, L., Ferreira, V.P., 2016. Timing and tectonic implications of the Pan-African Bangangte syenomonzonite, West Cameroon: constraints from in-situ zircon U–Pb age and Hf-O isotopes. J. Afric. Earth Sci. 124, 94–103.
Temdjim, R., 2012. Ultramafic xenoliths from Lake nyos area, Cameroon volcanic line, west-Central Africa: petrography, mineral chemistry, equilibration conditions and metasomatic features. Chem. Erde-Geochem. 72, 39–60.
Tedonkenfack, S.S.T., Tamen, J., Nkouathio, D.G., Asaah, A.N.E., Gountié, M.D., Aka, F. T., 2019. Petrography and geochemistry of mantle xenoliths from the Ibal-Oku region (North-West region, Cameroon): Preliminary evidence of mantle heterogeneities. Journal of African Earth Sciences 154 (2019), 70–79.
Teitchou, M., Grégoire, M., Temdjim, R., Ghogomu, R., Ngwa, C., Aka, F., 2011. Mineralogical and geochemical fingerprints of mantle metasomatism beneath nyos volcano (Cameroon volcanic line). Geol. Soc. Am. Spec. Pap. 478, 193–210.
Toteu, S.F., Michard, A., Bertrand, J.M., Rocci, G., 1987. U/pb dating of precambrian rocks from northern cameroon, orogenic evolution and chronology of the pan-african belt of central africa. Precambrian Res. 37 (1), 71–87.
Toteu, S.F., Garoua, Macaudiere J., Bertrand, J.M., Dautel, D., Nancy, 1990. Metamorphic zircons from North Cameroon; implications for the Pan-African evolution of Central Africa. Geol. Rundsch. 79 (3), 777–788. Stuttgart 1990.
Toteu, S.F., Van Schmus, W.R., Penaye, J., Michard, A., 2001. New U-Pb and Sm-Nd data from north-Central Cameroon and its bearing on the pre-pan African history of Central Africa. Precambrian Res. 108, 45–73.
Vicat, et al., 2001. Existence of old doleritic dykes of continental tholeiite composition, in the Cameroon Line alkaline province. Implication to the geodynamical context. Comptes Rendus de l'Académie des Sciences - Series IIA. Earth Planet. Sci. 332 (4), 243–249, 28 February 2001.
Wembenyui, E.W., Collerson, K.D., Zhao, J.-X., 2020. Evolution of Mount Cameroon volcanism: geochemistry, mineral chemistry and radiogenic isotopes (Pb, Sr, Nd). Geosci. Front. https://doi.org/10.1016/j.gsf.2020.03.015.
White, R., McKenzie, D., 1989. Magmatism at rift zones: the generation of volcanic continental margins and flood basalts. Journal of Geophysical Research: Solid Earth 94 (B6), 7685–7729, 1978–2012.
Wilson, M., 1992. Magmatism and continental rifting during the opening of the South Atlantic Ocean: a consequence of Lower Cretaceous super-plume activity?. In: Magmatism and the Causes of Continental Break-up Geological Society Special Publications, 68, pp. 241–255.
Xiong, F.H., Ma, C.Q., Jiang, H.A., Liu, B., Zhang, J.Y., Zhou, Q., 2013. Petrogenetic and tectonic significance of Permian calc-alkaline lamprophyres, East Kunlun orogenic belt, Northern Qinghai-Tibet Plateau. Int. Geol. Rev. https://doi.org/10.1080/00206814.2013.804683.
Yokoyama, T., Nagai, Y., Hinohara, Y., Mori, T., 2017. Investigating the influence of nonspectral matrix effects for determination of 22 trace elements in rock samples by ICP-QMS.
Yokoyama, T., Aka, F.T., Kusakabe, M., Nakamura, E., 2007. Plume–lithosphere interaction beneath mt. Cameroon volcano, West Africa: constraints from 238 U–230 Th–226 Ra and Sr–Nd–Pb isotope systematics. Geochim. Cosmochim. Acta 71, 1835–1854.
Yokoyama, T., Makishima, A., Nakamura, E., 1999. Separation of thorium and uranium from silicate rock samples using two commercial extraction chromatographic resins. Anal. Chem. 71, 135–141.